Geometric similarity on interparticle force evaluation for scaled-up DEM particles

Yuze Hu, Ei L. Chan, Takuya Tsuji, Toshitsugu Tanaka, Kimiaki Washino*

Department of Mechanical Engineering, Osaka University, Suita, Osaka 565-0871, Japan

Abstract

The scaled-up particle model, which is also commonly known as the coarse grain model or discrete parcel model, is frequently used to reduce the computational cost in Discrete Element Method (DEM). In the direct force scaling approach, the forces acting on original particles are first estimated and then directly scaled to apply to scaled-up particles. It is therefore crucial to appropriately evaluate the variables of the original particles, e.g. overlap and separation distance, from the scaled-up particles particularly when estimating complex interparticle forces. The present work proposes the use of geometric similarity for the evaluation of the original particle overlap and separation distance. It is demonstrated that the proposed method can provide an almost identical stress-strain curve between the original and scaled-up particles during uniaxial compression of a packed particle bed, whilst the conventional method in the literature gives significant overestimation of the stress. In addition, the scaled-up particles can reasonably replicate the original velocity

*Corresponding author. Tel.: +81-6-6879-7318.

Email address: washino.k@mech.eng.osaka-u.ac.jp (Kimiaki Washino)

distributions of cohesive particles with both liquid bridge and JKR surface adhesion forces in a dynamic flow system (vertical mixer). The simulation results suggest that the method proposed can be applied to any type of interparticle forces. A scaling of time step limit is also derived theoretically and discussed.
Keywords: DEM, Scaled-up particle model, Interparticle force, Geometric similarity, Calculation speed-up

1. Introduction

Powder handling processes can play a critical role in various industries. Particularly in the pharmaceutical industry, the size of primary particles is usually small and the particle level interactions can have a considerable impact on the macroscopic or bulk powder flow which can determine the quality of the final products. However, measuring particle interactions and internal behaviour of particles by experiment is challenging, and computer simulations can be a powerful alternative to gain more insight into these processes.

Discrete Element Method (DEM), which was first developed by Cundall and Strack [1] for soil mechanics, has been widely used to simulate powder flows. One of the most significant advantages of DEM over other simulation methods is its ability to directly consider the particle interactions. Previously, DEM was mostly used to simulate relatively coarse particles where only contact force [1, 2] and body (external) force [3, 4] are dominant due

to its simplicity, and proven to provide comparable results to experimental data [5, 6]. Recently, an increasing number of researchers are trying to incorporate more complex interparticle forces into DEM, such as capillary force [7, 8, 9, 10], viscous force [11, 12, 13, 14, 15], surface adhesion force [16, 17, 18, 19, 20], and electrostatic force [21, 22]. These attraction forces can cause agglomerates, lumps and/or wall make-ups, that are not observed with free-flowing particles.

One of the most significant problems of DEM is the extremely high computational cost to track the movement of a large number of particles. In general, far more than billions of particles can exist in industrial-scale equipment. Despite the rapid advancement of computational power over the past decades, it is still difficult or practically impossible to finish such large-scale simulation within an acceptable period of time. Therefore, various strategies have been applied to speed-up DEM simulation, such as GPU computing [23, 24, 25], domain decomposition [26, 27], reduced particle stiffness [28, 29, 30, 31, 32], and scaled-up particle model [33, 34, 35, 36, 37, 38]. Among them, the scaled-up particle model has been an increasingly popular approach where particle size is artificially increased to reduce the total number of particles in a system. It is also known as the coarse grain model or discrete parcel model. Although the term "coarse grain model" may be more common in this field [39, 40, 41, 42, 43], the same term is sometimes used to indicate the volume-averaging of discrete particle quantities in a continuous field in CFD–DEM coupling [44, 45]. In order to avoid the confusion, the

term "scaled-up particle model" is used in this paper. A good review for the current scaled-up particle models is provided by Di Renzo et al. [46].

In the scaled-up particle model, it is important to properly scale the forces acting on the scaled-up particles so that they represent the behaviour of original particles. Several models have been proposed in the literature, and Chan and Washino [37] classified them into two types: parameter scaling and direct force scaling. The parameter scaling adjusts the physical properties or DEM parameters to achieve kinematic similarity to the original particle system [34, 36]. This approach is fairly simple and does not require any additional coding for implementation. However, the scaling criterion of each parameter depends on the force models used and can be difficult or even impossible to determine for complex forms of forces. In the direct force scaling, the forces acting on original particles are first estimated using the original particle properties (e.g. particle stiffness and friction coefficient) and variables (e.g. particle overlap, separation distance and relative velocity), and then directly scaled to apply to scaled-up particles. This approach seems to be more versatile and easier to find generic scaling criteria.

In the direct force scaling, considering that l is the scale factor (i.e., the size ratio of the scaled-up to original particles), the pioneering work of Sakai and Koshizuka [33] proposed l^3 scaling for contact force, fluid force and gravitational force, i.e. the forces for the scaled-up particle are l^3 times larger than those estimated for the original particle. Sakai et al. [35] later employed l^2 scaling for cohesion force by maintaining the potential energy between the

original and scaled-up particles, whilst the l^3 scaling is still used for the other forces. Chan and Washino [37] proposed l^2 scaling for any interparticle force (e.g. contact force and liquid bridge force) and l^3 scaling for any body force (e.g. fluid force in the CFD–DEM framework and gravitational force) using the continuum assumption of a fully packed particles. More recently, it is theoretically proven that the same scaling is applicable to arbitrary flows by Washino et al. [38], which can provide promising results for complex systems such as gas-liquid-solid three-phase flows.

In the scaled-up particle model, the original particles are not explicitly simulated but represented by scaled-up particles. Therefore, particularly in the direct force scaling, it is important to properly evaluate the original particle variables related to the force estimation, such as the translational velocity, angular velocity, particle overlap and separation distance, from the corresponding scaled-up particle variables. Sakai and Koshizuka [33] suggested to use the same translational velocity between the original and scaled-up particles, whilst the angular velocity of the original particle is taken to be l times larger than that of the scaled-up particle. These relationships are based on the conservation of the total kinetic energies in both the original and scaled-up particle systems. On the other hand, they assumed that the overlap of the original particle is the same as that of the scaled-up particle when estimating the contact force, which is not as well-grounded in theory. The same assumption is employed by Chan and Washino [37] for the separation distance to estimate the liquid bridge forces. However, to the best

of the authors' knowledge, the validity of these assumptions is not properly discussed in the literature.

The present study attempts to obtain a deeper understanding of the direct force scaling approach in the scaled-up particle model. Particularly, it focuses on the evaluation of original particle variables and we propose to use geometric similarity for both particle overlap and separation distance, i.e. they are scaled by the scale factor l to ensure the same amount of mass to be accommodated in a fixed space. Simulations of contact dominant uniaxial compression of a packed particle bed as well as wet and cohesive particle flows in a vertical mixer are presented to discuss the validity of the proposed method.

2. Discrete Element Method

2.1. Governing equations

Equations of translational and rotational motion of Particle i interacting with adjacent Particle j are given by Equations (1) and (2):

$$m_i \dot{\boldsymbol{v}}_i = \sum_j \boldsymbol{F}_{Iij} + \boldsymbol{F}_{Bi} \tag{1}$$

$$I_i \dot{\boldsymbol{\omega}}_i = \sum_j \boldsymbol{M}_{Iij} \tag{2}$$

where m is the particle mass, $\boldsymbol{v}$ is the translational velocity, I is the moment of inertia, $\boldsymbol{\omega}$ is the angular velocity, $\boldsymbol{F}$ is the force and $\boldsymbol{M}$ is the torque

acting on the particle. The forces acting on the particles can be generically represented by interparticle force, $\boldsymbol{F}_I$, and body force, $\boldsymbol{F}_B$. The interparticle force may consist of contact force, $\boldsymbol{F}_C$, and attraction force, $\boldsymbol{F}_A$, as:

$$\boldsymbol{F}_I = \boldsymbol{F}_C + \boldsymbol{F}_A \tag{3}$$

The attraction force can be capillary, viscous, surface adhesion and electrostatic forces. The body force typically includes gravitational force and fluid force in the CFD–DEM framework. $\boldsymbol{M}_I$ is the torque due to the interparticle force and defined as:

$$\boldsymbol{M}_I = r\boldsymbol{n} \times \boldsymbol{F}_I \tag{4}$$

where r is the particle radius and $\boldsymbol{n}$ is the unit normal vector.

The force models used for the validation study in this work are briefly explained below. However, it is important to stress that the scaled-up particle model discussed in Section 3 is not limited to them and applicable to any force model in principle.

2.2. Contact force

The contact forces in the normal and tangential directions are given by:

$$\boldsymbol{F}_{Cn} = -\left(\frac{4E^*}{3r^*}a^3 + \eta_n \boldsymbol{v}_{rel} \cdot \boldsymbol{n}\right)\boldsymbol{n} \tag{5}$$

$$\boldsymbol{F}_{Ct} = -\min(8G^*\sqrt{r^*\delta_n}\delta_t + \eta_t v_s,\ \mu_s F_N)\boldsymbol{t} \tag{6}$$

where a is the contact radius, δ is the particle overlap (i.e. particle deformation), η is the damping coefficient, $\boldsymbol{v}_{rel}$ is the relative velocity, v_s is the magnitude of the relative tangential velocity at the contact surface, μ_s is the sliding friction coefficient, F_N is the normal load during sliding and $\boldsymbol{t}$ is the unit tangent vector. The subscripts $_n$ and $_t$ indicate the quantities for the normal and tangential directions, respectively. r^*, E^* and G^* are defined as:

$$\frac{1}{r^*} = \frac{1}{r_i} + \frac{1}{r_j} \tag{7}$$

$$\frac{1}{E^*} = \frac{1-\nu_i^2}{E_i} + \frac{1-\nu_j^2}{E_j} \tag{8}$$

$$\frac{1}{G^*} = \frac{2(2-\nu_i)(1+\nu_i)}{E_i} + \frac{2(2-\nu_j)(1+\nu_j)}{E_j} \tag{9}$$

where E is the Young's modulus and ν is the Poisson's ratio. In the Hertzian theory, the contact radius a is calculated as:

$$a = \sqrt{r^* \delta_n} \tag{10}$$

In the JKR theory, a is given as the solution of the following equation [47]:

$$a^4 - 2r^*\delta_n a^2 - \frac{4\pi\gamma r^{*2}}{E^*} a + r^{*2}\delta_n^2 = 0 \tag{11}$$

where γ is the surface energy of the particle. The damping coefficients in the normal and tangential directions are given as [2]:

$$\eta_n = -2\sqrt{\frac{5}{3}}\beta(m^*E^*)^{1/2}r^{*1/4}\delta_n^{1/4} \tag{12}$$

$$\eta_t = -4\sqrt{\frac{5}{3}}\beta(m^*G^*)^{1/2}r^{*1/4}\delta_n^{1/4} \tag{13}$$

$$\frac{1}{m^*} = \frac{1}{m_i} + \frac{1}{m_j} \tag{14}$$

where β is a function of the coefficient of restitution, e, and defined as:

$$\beta = \frac{\ln(e)}{\sqrt{\ln^2(e) + \pi^2}} \tag{15}$$

F_N is given by the magnitude of the normal contact force when the Hertzian theory is used. In the JKR theory, it is given by the effective normal force as [48, 49]:

$$F_N = \left| 4\left(\frac{a}{a_0}\right)^3 - \left(\frac{a}{a_0}\right)^{3/2} + 2 \right| F_{po} \tag{16}$$

where F_{po} is the pull-off force and a_0 is the contact radius at the equilibrium condition, which are defined as:

$$F_{po} = 3\pi\gamma r^* \tag{17}$$

$$a_0 = \left(\frac{9\pi\gamma r^{*2}}{E^*}\right)^{1/3} \tag{18}$$

2.3. Attraction force

Various models for attraction force, $\boldsymbol{F}_A$, have been proposed and applied in DEM such as capillary force [7, 8, 9, 10], viscous force [11, 12, 13, 14, 15], surface adhesion force [16, 17, 18, 19, 20], and electrostatic force [21, 22]. The capillary force and JKR surface adhesion force are used in this work, which are summarised below.

2.3.1. Capillary force model

When a small amount of liquid is dispersed in particles, liquid bridges may be formed which creates capillary forces between the particles. The liquid bridges are typically assumed to be symmetrical and pendular in shape. There are two approaches for modelling capillary force: the Laplace and energetic approaches [10], and many models are available in the literature [7, 8, 9, 10, 50]. The Rabinovich-Lambert model [9, 10] is used in the present work, which is given as:

$$\boldsymbol{F}_{cap} = C_{cap}\boldsymbol{n} \tag{19}$$

$$C_{cap} = \frac{4\pi r^* \sigma \cos\theta}{1 + 1/(\sqrt{1 + V_{liq}/\pi r^* S^2} - 1)} \tag{20}$$

where V_{liq} is the liquid bridge volume, σ is the surface tension, θ is the contact angle and S is the separation distance. A lower cut-off value of the separation distance, S_{min}, is employed to avoid S from being excessively small or negative during particle contact. The upper cut-off value is given

by the following rupture distance [51]:

$$S_{rup} = (1 + 0.5\theta)V_{liq}^{1/3} \tag{21}$$

A liquid bridge is formed when the surfaces of two approaching particles come into contact, and then breaks when the separation distance reaches the rupture distance. Note that the pendular liquid bridge model used is only valid when the liquid to solid volume ratio is small. Therefore, it can be assumed that the thickness of the liquid film on the particle surface is much smaller than the size of particles and ignored in the approaching stage.

2.3.2. JKR surface adhesion force model

Many models have been proposed to explain the surface adhesion force [16, 17, 18] which commonly make use of the surface energy. One of the most frequently used models in DEM is based on the JKR theory [16, 19, 20, 28, 47], which is valid when the following dimensionless Tabor parameter, λ_T, is sufficiently large [52]:

$$\lambda_T = \left(\frac{4r^*\gamma^2}{E^{*2}D_{min}^3} \right)^{1/3} \tag{22}$$

where D_{min} is the minimum atomic separation distance between the particles. In the JKR theory, the normal adhesion force is calculated by:

$$\boldsymbol{F}_{JKR} = 4\sqrt{\pi\gamma E^* a^3}\boldsymbol{n} \tag{23}$$

In the original JKR model, this force can be exerted until the contact breaks during the separation process with negative overlap. A simplified model used in many studies [53, 47, 28] is employed in this work where the contact is assumed to be broken as soon as the normal overlap becomes negative.

3. Scaled-up particle model

In the scaled-up particle model, the size of particles used in simulation is artificially increased while keeping the system size so that the computational cost is reduced. Hereafter, the system with original particle size is called "original system" whereas that with increased particle size is called "scaled-up system". The latter should not be confused with the scale-up of a system itself (often seen in an industrial process) which increases the system size while keeping the particle size. l is defined as a scale factor, i.e. the size ratio of the scaled-up to original particles:

$$l = d_{\mathrm{S}}/d_{\mathrm{O}} \tag{24}$$

where d is the particle diameter and the subscripts $_{\mathrm{O}}$ and $_{\mathrm{S}}$ indicate the original and scaled-up systems, respectively.

3.1. Scale power index

In the direct force scaling approach, the force and torque applied on the scaled-up particle are l^m times larger than those of the original particle where m is called the scale power index. Several scale power indices have already

been proposed in the literature. Sakai and Koshizuka [33] proposed $m = 3$ for the contact, fluid and gravitational forces to keep the same equations of motion between the original and scaled-up systems in the particle level. In other words, the same scale power index is applied to both interparticle and body forces:

$$\boldsymbol{F}_{I\mathrm{S}} = l^3 \boldsymbol{F}_{I\mathrm{O}} \tag{25}$$

$$\boldsymbol{F}_{B\mathrm{S}} = l^3 \boldsymbol{F}_{B\mathrm{O}} \tag{26}$$

$m = 4$ is assigned to the contact torque in their formulation as:

$$\boldsymbol{M}_{I\mathrm{S}} = r_{\mathrm{S}} \boldsymbol{n} \times \boldsymbol{F}_{I\mathrm{S}} = l r_{\mathrm{O}} \boldsymbol{n} \times l^3 \boldsymbol{F}_{I\mathrm{O}} = l^4 \boldsymbol{M}_{I\mathrm{O}} \tag{27}$$

Sakai et al. [35] inherited the same indices except that $m = 2$ is used for the van der Waals force to maintain the same potential energy. Their scale power indices are summarised in Table 1.

[Table 1 about here.]

Chan and Washino [37] proposed more generic indices, i.e. $m = 2$ for any interparticle force and $m = 3$ for any body force as:

$$\boldsymbol{F}_{I\mathrm{S}} = l^2 \boldsymbol{F}_{I\mathrm{O}} \tag{28}$$

$$\boldsymbol{F}_{B\mathrm{S}} = l^3 \boldsymbol{F}_{B\mathrm{O}} \tag{29}$$

These relationships are derived from the continuum assumption of fully

packed particles where the forces acting on control volumes are kept the same between the original and scaled-up systems. It is theoretically proven by Washino et al. [38] that the same indices can be applied to more generalised particle flows. Using the same concept, $m = 2$ should be applied to any interparticle torque as:

$$\boldsymbol{M}_{I\mathrm{S}} = l^2 \boldsymbol{M}_{I\mathrm{O}} \tag{30}$$

Their scale power indices are summarised in Table 2.

[Table 2 about here.]

3.2. Evaluation of original particle variables

In scaled-up particle simulation, original particles are not explicitly used but represented by scaled-up particles. Therefore, it is crucial to accurately evaluate the original particle variables from those of the scaled-up particle to estimate the forces acting on the original particles. These variables include the particle translational velocity, angular velocity, particle overlap and separation distance. Sakai and Koshizuka [33] suggested that the translational velocity of the original particle should be the same as that of the scaled-up particle from the translational kinetic energy point of view:

$$\boldsymbol{v}_{\mathrm{O}} = \boldsymbol{v}_{\mathrm{S}} \tag{31}$$

It is also proven that the same translational velocity maintains the convective momentum flux across the faces of control volumes by Washino et al. [38]. The angular velocity is scaled by l to keep the same rotational kinetic energy between the original and scaled-up systems:

$$\boldsymbol{\omega}_{\mathrm{O}} = l\boldsymbol{\omega}_{\mathrm{S}} \tag{32}$$

These relationships for velocities have a solid theoretical basis and seem to be reasonable. In contrast, the evaluation methods of particle overlap and separation distance are not well-grounded. Sakai and Koshizuka [33] assumed that the overlap of the original particle is the same as that of the scaled-up particle, and Chan and Washino [37] employed the same idea for separation distance, that is:

$$\delta_{\mathrm{O}} = \delta_{\mathrm{S}} \tag{33}$$

$$S_{\mathrm{O}} = S_{\mathrm{S}} \tag{34}$$

It is suggested in this work that the overlap and separation distance should be calculated using geometric similarity:

$$\delta_{\mathrm{O}} = \delta_{\mathrm{S}}/l \tag{35}$$

$$S_{\mathrm{O}} = S_{\mathrm{S}}/l \tag{36}$$

The key of the scaled-up particle model proposed is to keeping the same flows in the control volume level between the original and scaled-up systems. In the continuum assumption, any quantities in the control volumes are expected to be homogeneous. Assuming the homogeneous structure of particles in Figure 1, Equations (35) and (36) are required to accommodate the same mass in the control volume, i.e. $m_{\mathrm{O}}n^3 = m_{\mathrm{S}}n^3/l^3$, where n is the number of particles aligned in one dimension. The relationships of the variables between the original and scaled-up particles are summarised in Table 3.

Additionally, for wet particle cases, the liquid bridge volume for the original particle is evaluated as [37]:

$$V_{liq\mathrm{O}} = V_{liq\mathrm{S}}/l^3 \tag{37}$$

The rupture distance, S_{rup}, is calculated using $V_{liq\mathrm{O}}$, and the liquid bridge ruptures when the separation distance given by Equation (36) is larger than S_{rup}. Similarly, the minimum separation distance, S_{min}, should be determined based on the asperity of the original particle surface, and when the separation distance given by Equation (36) is smaller than S_{min}, the minimum separation distance is used to calculate the capillary force.

[Figure 1 about here.]

[Table 3 about here.]

3.3. Scaling of time step

In this section, a head-on collison of two particles is considered to discuss the scaling of the stable time step. When two original particles are in contact, the equation of motion can be writtern using the Hertzian contact theory as:

$$m_{\mathrm{O}}^{*}\frac{dv_{r\mathrm{O}}}{dt} = -\frac{4}{3}E^{*}r_{\mathrm{O}}^{*1/2}\delta_{\mathrm{O}}^{3/2} \tag{38}$$

where v_r is the relative velocity and δ is the normal overlap. Since the time step in DEM is usually determined based on the contact force alone in the literature [3, 6], any cohesion force is ignored here for simplicity. Employing the l^2 scaling law and geometric similarity explained above, the equation of motion for two colliding scaled-up particles is given as:

$$m_{\mathrm{S}}^{*}\frac{dv_{r\mathrm{S}}}{dt} = -l^2\frac{4}{3}E^{*}r_{\mathrm{O}}^{*1/2}\left(\frac{\delta_{\mathrm{S}}}{l}\right)^{3/2} \tag{39}$$

Rearranging Equation (39) gives:

$$m_{\mathrm{S}}^{*}\frac{dv_{r\mathrm{S}}}{dt} = -\frac{4}{3}E^{*}r_{\mathrm{S}}^{*1/2}\delta_{\mathrm{S}}^{3/2} \tag{40}$$

Since Equations (38) and (40) are written in the same form, the same expression for the time step can be used. Typically, with the Hertzian theory, the time step is given by the Rayleigh time [6], that is proportional to the particle size:

$$\Delta t \sim \frac{\pi r}{0.8766 + 0.163\nu}\sqrt{\frac{2\rho(1+\nu)}{E}} \tag{41}$$

Therefore, the time step for the scaled-up particle can be l times larger than that of the original particle.

4. Results and discussion

Several simulations are performed to discuss the validity of the scale power index and the evaluation of original particle variables explained in Section 3. In each system presented in this section, three different methods for scaled-up particles are tested as summarised in Table 4. Following Chan and Washino [37], different scale power indices are used for interparticle and body forces. Method 1 uses $m = 2$ for both interparticle forces and torques in conjunction with the geometric similarity to evaluate the particle overlap and separation distance, while $m = 3$ is used for body force. This is the method suggested in the present work. Method 2 uses the same scale power indices as Method 1 but the original particle overlap and separation distance are assumed to be the same as those of the scaled-up particle (i.e. the conventional method). Method 3 uses $m = 3$ for both interparticle and body forces (similar to Sakai and Koshizuka's model) as well as the corresponding torques with geometric similarity for the evaluation of the original variables.

[Table 4 about here.]

4.1. Uniaxial compression of packed particle bed

The first validation test is uniaxial compression of packed particles as shown in Figure 2. The original particle properties used are listed in Table 5.

The original particle diameter is 0.5 mm and density is 2500 kg/m^3. Particles with diameters of 1 and 2 mm are employed as scaled-up particles, i.e. the scale factors of 2 and 4, respectively.

[Figure 2 about here.]

[Table 5 about here.]

The initial particle beds are prepared using the following steps. Particles with small sliding friction ($\mu_s = 0.01$) are randomly generated and allowed to fall into the simulation domain with dimensions of $14 \times 14 \times 200$ mm^3 by gravity. A plane wall is placed at the bottom and periodic boundaries are used in the lateral directions. The low friction particles are used to make the initial particle beds compact. Then the particles above 100 mm from the bottom are removed and an upper wall is placed at the bed surface.

During the compression process, the sliding friction coefficient is reset to 0.3. The upper wall is moved downwards with a constant speed of 5 mm/s while the bottom wall is fixed in space. The bed is compressed until the upper wall moves 10 mm, i.e. strain of 0.1. The stress on the upper wall is monitored during the compression. No attraction force is considered and the contact force is calculated using the Hertzian theory. Although gravitational force is exerted on the particles, it only has a negligible impact on the stress obtained.

Figure 3 shows the stress-strain relationship obtained from the simulations. It can be seen in Figure 3(a) that the results of the original and

scaled-up particles with Method 1 almost fall into the same curve. On the other hand, in Figure 3(b) and (c), the scaled-up particles significantly overestimate the compression stress, and this tendency is more pronounced as the scale factor increases. It is concluded from these simulations that the l^2 scaling with the geometric similarity for particle overlap is the most appropriate method for a contact force dominant system.

[Figure 3 about here.]

4.2. Particle flow in a vertical mixer

The second validation test is a dynamic system of particle flow in a vertical mixer where attraction forces are exerted on the particles. The mixer used is a scaled-down version of the 10L Roto Junior high shear granulator (Zanchetta Lucca). The inner diameter of the mixer is 84 mm and a 3-bladed impeller shown in Figure 4 is mounted at the bottom. The common properties of the original particles used in all cases are listed in Table 6. The original particle diameter is 0.5 mm, density is 1000 kg/m^3, and the total mass is 0.0458 kg as used by Chan and Washino [37]. The impeller rotates with 300 rpm until the flow reaches steady state. Particles with diameters of 1 and 2 mm are employed as scaled-up particles, i.e. scale factors of 2 and 4, respectively. Although it is possible to further increase the particle size, the mixer to particle diameter ratio, D/d, should not be too small in order to minimise boundary effects [54, 55]. The range of D/d in this study is from 42 to 168 which is in accordance with the recommendation of $D/d \geq 40$ in

the literature [54, 55]. More results and discussions about the D/d ratio can be found in Appendix.

[Figure 4 about here.]

[Table 6 about here.]

Two sets of simulations are carried out and presented in Sections 4.2.1 and 4.2.2, respectively, with different combinations of contact and attraction force models. The first is the Hertzian contact with the capillary force model explained in Section 2.3.1, and the second is the JKR adhesive contact model explained in Section 2.3.2. The attraction forces between the particles and mixer walls are deactivated so that the particles do not adhere to the casing wall and impeller, which may reduce the amount of bulk moving particles available for velocity analyses.

4.2.1. Wet particles with capillary force

The particles are assumed to be uniformly wet with liquid. The liquid to solid volume ratio is 0.05 and does not change with time. 8.3 % of the liquid on the particle surface is used for the formation of the bridge between each particle pair so that the entire liquid is used in the case of maximum packing, i.e.:

$$V_{liq} = 0.083 \times 0.05 \times (V_{pi} + V_{pj}) \tag{42}$$

where V_p is the particle volume. Four different values of surface tension coefficient are tested, i.e. 0.05, 0.1, 0.2 and 0.4 N/m. The contact angle

is set to 0 deg and viscous force is not taken into account. The minimum separation distance used is 1 μm.

Figure 5 shows snapshots of the original particle flow with different values of surface tension. It is a typical flow of cohesive particles that particles are bonded together and form lumps. The size of the lumps increases as the surface tension increases. Especially with $\sigma = 0.4$ N/m, the entire particles are lumped together. The overall particle velocity increases as the surface tension increases. This is because the relative velocity of the large lumps to the impeller is smaller than that of the small lumps.

[Figure 5 about here.]

Figures 6 and 7 show snapshots of the scaled-up particle flow using Method 1 with scale factors of 2 and 4, respectively. Although the boundaries of the lumps become less clear as the scale factor increases (especially with $\sigma = 0.1$ and 0.2 N/m), the overall flow structure and velocity field of the original particles are well captured. Figures 8 and 9 show snapshots of the scaled-up particles using Method 2 with scale factors of 2 and 4, respectively. The overall flow structure is similar to that of the original particles to a certain extent. However, the boundaries of the lumps are even less clear compared to Method 1. In addition, comparing with Figure 5, the powder velocity in Figures 8 and 9 is smaller. It indicates that Method 2 cannot provide sufficiently large capillary force. Figures 10 and 11 show particle snapshots using Method 3 with scale factors of 2 and 4, respectively. It can

be clearly seen that the particles become more cohesive than the original particles, which indicates that Method 3 largely overestimates the capillary force.

[Figure 6 about here.]

[Figure 7 about here.]

[Figure 8 about here.]

[Figure 9 about here.]

[Figure 10 about here.]

[Figure 11 about here.]

Figures 12, 13 and 14 show the probability density distribution of the particle velocity magnitude at steady state with Methods 1, 2 and 3, respectively. The distribution without attraction force (i.e. $\sigma = 0$ N/m) is also included to indicate that the capillary force has a large impact on the particle velocity even with the smallest surface tension coefficient tested. First, we discuss the change of the original particle results with different surface tension values. When $\sigma = 0.05$ N/m, the distribution of the original particle velocity is narrow with a large peak value at around 0.75 m/s. The distribution becomes broader as the surface tension coefficient increases while the peak velocity is shifted rightward. When $\sigma = 0.4$ N/m, the probability increases linearly with the particle velocity, which indicates that almost the

entire particles move together with the impeller since a large lump is formed as can be seen in Figure 5(d).

Now, we compare the results of the original and scaled-up particles. In Figure 12, it can be seen that the scaled-up particles can reasonably reproduce the original particle velocity distribution. However, a slight discrepancy is observed when $\sigma = 0.1$ and 0.2 N/m due to the formation of the medium size lumps of the original particles, which cannot be "resolved" with the large scaled-up particles. In Figure 13, the peak velocities of the scaled-up particles are shifted leftwards from those of the original particles. This is because the capillary force is underestimated with the conventional evaluation of the separation distance. Finally, in Figure 14, the results obtained from the scaled-up particles are significantly different from the original particle results and the peak velocities are shifted rightwards. This is because the capillary force is largely overestimated with the l^3 scaling. In Figure 14(d), one may find the velocity distributions similar between the original and scaled-up systems. However, this is simply because all the particles form a single lump due to the strong capillary force above which the velocity distribution does not change any more. Note that the results of the scaled-up particles in Figure 14(c) and (d) are almost the same. It is concluded from these simulations that the l^2 scaling with geometric similarity is the most appropriate method to replicate the original particle behaviour in a capillary force dominant system.

[Figure 12 about here.]

[Figure 13 about here.]

[Figure 14 about here.]

The influence of the liquid content is crucial in many wet particle handling processes. For further validating the scaled-up particle model proposed, simulations with liquid to solid volume ratio of 0.005 are also performed. The surface tension used is $\sigma = 0.05$ N/m and the other conditions are exactly the same as the simulations above. Figure 15 shows the probability density distribution of the particle velocity of the original and scaled-up ($l = 4$) systems. The peak velocity is shifted leftward by decreasing the liquid volume since the both capillary force and rupture distance become small. It can be seen that the proposed model can well capture the sensitivity of the original particle velocity to the liquid volume.

[Figure 15 about here.]

4.2.2. Particles with JKR adhesion force

It is considered that the surface adhesion force calculated from the simplified JKR model is exerted on the particles. Four different values of surface energy are tested, i.e. 0.1, 0.2, 0.4 and 0.8 J/m^2. Since the original particle size is relatively large (0.5 mm), artificially large surface energy values are used so that noticeable impacts on the particle velocity can be seen. Note that the purpose of these tests is to discuss the validity of the scaled-up particle model.

Figures 16, 17 and 18 show the probability density distribution of the particle velocity magnitude at steady state with Methods 1, 2 and 3, respectively. Similar to the capillary force cases discussed in Section 4.2.1, it can be seen that Method 1 provides the best prediction of the original particle velocity whilst Methods 2 and 3 give much larger differences. This proves that the l^2 scaling with the geometric similarity for particle overlap is valid for a system where surface adhesion force is dominant. The results presented in Sections 4.1, 4.2.1 and 4.2.2 implies that the proposed method is versatile and universally applicable for any type of interparticle force.

[Figure 16 about here.]

[Figure 17 about here.]

[Figure 18 about here.]

4.3. Particles in a periodic box

Simulations of particles in a periodic box are conducted to verify the linear scaling of time step presented in Section 3.3. The properties of the original particles used are shown in Table 7. Cohesionless particles with diameter of 0.5 mm are randomly generated in a cubic domain with an edge length of 20 mm. Periodic boundary conditions are applied in all dimensions. The direction of the initial velocity of all particles is random and the magnitude is fixed to 1 m/s. The restitution coefficient is 1 and the sliding friction

coefficient is 0 so that there is no energy dissipation by the particle collisions. Particles of 1 and 2 mm in diameter are employed as the scaled-up particles using Method 1 in Table 4. In the scaled-up particle cases, the domain size is increased proportionally to the scale factor so that the same number of particles are accommodated in the simulation domain with the same packing fraction. The simulations are performed with different Δt to find the stable time step limit.

Figure 19 shows the temporal change of the total kinetic energy in the original particle case with $\Delta t = 0.2$, 0.5, 0.8 and 1 μs. Theoretically, although the total kinetic energy can fluctuate around a fixed value since a part of it is continuously converted to the potential energy of the spring between particles and vice versa, the energy of the perfectly elastic and frictionless particles never increases nor decreases with time. However, it can be seen that the total kinetic energy unphysically increases with time when $\Delta t = 0.8$ and 1 μs. This indicates that they are larger than the critical time step to resolve the collision event.

Figure 20 shows the increase rate of the total kinetic energy as a function of Δt in the original and scaled-up systems. In the original system, the energy increase rate becomes positive (i.e. unstable) when the time step is larger than approximately 0.6 μs. In the 1 and 2 mm particle cases, the critical time steps are approximately 1.2 and 2.4 μs, respectively, which are linear to the scale factor as discussed in Section 3.3.

[Table 7 about here.]

[Figure 19 about here.]

[Figure 20 about here.]

5. Conclusions

In the present work, a scaled-up particle model based on the direct force scaling is proposed to reduce the computational cost in DEM simulation. The particle overlap and separation distance of original particles are evaluated from the corresponding scaled-up particle variables using geometric similarity, which is different from the conventional method in the literature. The translational and rotational velocities are determined in such a way that the same kinetic energies can be achieved between the original and scaled-up particles as suggested by Sakai and Koshizuka [33]. Following Chan and Washino's [37] work, l^2 scaling is employed for any interparticle force and l^3 scaling for any body (external) force. Several validation simulations are carried out with Hertzian contact force, capillary force and JKR surface adhesion force.

It is shown that the proposed method can provide an almost identical stress-strain curve with that of the original system during the uniaxial compression of a packed particle bed, where particle contact forces are dominant. The same method can also reasonably reproduce the overall flow structure and velocity distributions of the original particles in a dynamic system (vertical mixer), where capillary and JKR surface adhesion forces are dominant. Slight discrepancies are observed when the attraction forces are relatively

large, which may be because of the formation of medium size lumps which cannot be resolved with large scaled-up particles. The method proposed can be applied to any type of interparticle force in principle, and it is proven by the simulation results presented. The linear correlation of the stable time step limit to the scale factor is theoretically derived in this work and demonstrated by the simulations of the perfectly elastic and frictionless particles.

Acknowledgements

The authors are grateful to JSPS (KAKENHI Grant No. 20K11850) for the financial support to this work. This research was supported in part through computational resources provided by Research Institute for Information Technology, Kyushu University.

Appendix

In general, for the particles flow in a mixer, it is recommended to use $D/d > 40$ to avoid the boundary effects [54, 55]. This may limit the selection of the scale factor: employing an excessively large scale factor may cause insufficient "resolution" to capture the original overall flows. In this appendix, several simulations are presented to discuss the valid range of the scale factor. The original simulation conditions are exactly the same as those used in Section 4.2.1 with $\sigma = 0.05$ N/m, and scaled-up particle diameters of 1, 2, 4 and 8 mm are employed, i.e. $D/d = 84$, 42, 21 and 10.5, respectively, using Method 1 in Table 4. Figure 21 shows the probability distribution of

the particles velocity obtained. It is clear that the peak velocities with 1 and 2 mm particles are almost the same and agree well with that of the original particle. However, the peak velocity is shifted leftward and the distribution becomes broader as the scale factor is further increased. From these results, it can be concluded that $D/d > 40$ is required to obtain consistent results without the boundary effects.

[Figure 21 about here.]

References

[1] P. A. Cundall, O. D. L. Strack, Discrete numerical model for granular assemblies, Geotechnique 29-1 (1979) 47–65. doi:10.1680/geot.1979.29.1.47.

[2] Y. Tsuji, T. Tanaka, T. Ishida, Lagrangian numerical simulation of plug flow of cohesionless particles in a horizontal pipe, Powder Technology 71 (1992) 239–250. doi:10.1016/0032-5910(92)88030-L.

[3] Y. Tsuji, T. Kawaguchi, T. Tanaka, Discrete particle simulation of two-dimensional fluidized bed, Powder Technology 77 (1993) 79–87. doi:10.1016/0032-5910(93)85010-7.

[4] R. Beetstra, M. A. van der Hoef, J. A. Kuipers, Numerical study of segregation using a new drag force correlation for polydisperse systems derived from lattice-boltzmann simulations, Chemical Engineering Science 62 (2007) 246–255. doi:10.1016/j.ces.2006.08.054.

[5] R. L. Stewart, J. Bridgwater, Y. C. Zhou, A. B. Yu, Simulated and measured flow of granules in a bladed mixer- a detailed comparison, Chemical Engineering Science 56 (2001) 5457–5471. doi:10.1016/S0009-2509(01)00190-7.

[6] Y. Li, Y. Xu, C. Thornton, A comparison of discrete element simulations and experiments for 'sandpiles' composed of spherical particles, Powder Technology 160 (2005) 219–228. doi:10.1016/j.powtec.2005.09.002.

[7] T. Mikami, H. Kamiya, M. Horio, Numerical simulation of cohesive powder behavior in a fluidized bed, Chemical Engineering Science 53 (1998) 1927–1940. doi:10.1016/S0009-2509(97)00325-4.

[8] Y. Muguruma, T. Tanaka, Y. Tsuji, Numerical simulation of particulate flow with liquid bridge between particles (simulation of centrifugal tumbling granulator), Powder Technology 109 (2000) 49–57, ¡b¿From Duplicate 2 (¡i¿Numerical Simulation of Particulate Flow with Liquid Bridge Between Particles (Simulation of Centrifugal Tumbling Granulator)¡/i¿ - Muguruma, Yoshitsugu; Tanaka, Toshitsugu; Tsuji, Yutaka)¡br/¿¡/b¿¡br/¿Liquid bridge calculation method (Contact angle is zero). doi:10.1016/S0032-5910(99)00226-0.

[9] Y. I. Rabinovich, M. S. Esayanur, B. M. Moudgil, Capillary forces between two spheres with a fixed volume liquid bridge: Theory and experiment, Langmuir 21 (2005) 10992–10997. doi:10.1021/la0517639.

[10] P. Lambert, A. Chau, A. Delchambre, S. Régnier, Comparison between two capillary forces models, Langmuir 24 (2008) 3157–3163. doi:10.1021/la7036444.

[11] M. J. Adams, V. Perchard, The cohesive forces between particles with interstitial liquid, Institute of Chemical Engineering Symposium 91 (1985) 147–160.

[12] A. J. Goldman, R. G. Cox, H. Brenner, Slow viscous motion of a sphere parallel to a plane wall-i motion through a quiescent fluid, Chemical Engineering Science 22 (1967) 637–651. doi:10.1016/0009-2509(67)80047-2.

[13] O. Pitois, P. Moucheront, X. Chateau, Liquid bridge between two moving spheres: An experimental study of viscosity effects, Journal of Colloid and Interface Science 231 (2000) 26–31. doi:10.1006/jcis.2000.7096.

[14] K. Washino, E. L. Chan, T. Matsumoto, S. Hashino, T. Tsuji, T. Tanaka, Normal viscous force of pendular liquid bridge between two relatively moving particles, Journal of Colloid and Interface Science 494 (2017) 255–265. doi:10.1016/j.jcis.2017.01.088.

[15] K. Washino, E. L. Chan, H. Midou, T. Tsuji, T. Tanaka, Tangential viscous force models for pendular liquid bridge of newtonian fluid between moving particles, Chemical Engineering Science 174 (2017) 365–373. doi:10.1016/j.ces.2017.09.028.

[16] K. L. Johnson, K. Kendal, A. D. Roberts, Surface energy and the contact of elastic solids, Proceedings of the Royal Society of London. A. Mathematical and Physical Sciences 324 (1971) 301–313. doi:10.1098/rspa.1971.0141.

[17] B. V. Derjaguin, V. M. Muller, Y. P. Toporov, Effect of contact deformations on the adhesion of particles, Progress in Surface Science 45 (1994) 131–143. doi:10.1016/0079-6816(94)90044-2.

[18] D. Maugis, Adhesion of spheres: The jkr-dmt transition using a dugdale model, Journal of Colloid And Interface Science 150 (1992) 243–269. doi:10.1016/0021-9797(92)90285-T.

[19] B. K. Mishra, C. Thornton, Impact breakage of particle agglomerates, International Journal of Mineral Processing 61 (2001) 225–239. doi:10.1016/S0301-7516(00)00065-X.

[20] A. Hassanpour, S. J. Antony, M. Ghadiri, Effect of size ratio on the behaviour of agglomerates embedded in a bed of particles subjected to shearing: Dem analysis, Chemical Engineering Science 62 (2007) 935–942. doi:10.1016/j.ces.2006.10.026.

[21] J. Yang, C. Y. Wu, M. Adams, Dem analysis of the effect of electrostatic interaction on particle mixing for carrier-based dry powder inhaler formulations, Particuology 23 (2015) 25–30. doi:10.1016/j.partic.2014.12.007.

[22] C. Pei, C. Y. Wu, M. Adams, Dem-cfd analysis of contact electrification and electrostatic interactions during fluidization, Powder Technology 304 (2016) 208–217. doi:10.1016/j.powtec.2016.08.030.

[23] N. Govender, D. N. Wilke, C. Y. Wu, R. Rajamani, J. Khinast, B. J. Glasser, Large-scale gpu based dem modeling of mixing using irregularly shaped particles, Advanced Powder Technology 29 (2018) 2476–2490. doi:10.1016/j.apt.2018.06.028.

[24] Y. He, T. J. Evans, A. B. Yu, R. Y. Yang, A gpu-based dem for modelling large scale powder compaction with wide size distributions, Powder Technology 333 (2018) 219–228. doi:10.1016/j.powtec.2018.04.034.

[25] Y. He, F. Muller, A. Hassanpour, A. E. Bayly, A cpu-gpu cross-platform coupled cfd-dem approach for complex particle-fluid flows, Chemical Engineering Science 223 (2020) 115712. doi:10.1016/j.ces.2020.115712.

[26] T. Tsuji, K. Yabumoto, T. Tanaka, Spontaneous structures in three-dimensional bubbling gas-fluidized bed by parallel dem-cfd coupling simulation, Powder Technology 184 (2008) 132–140, cited By 92. doi:10.1016/j.powtec.2007.11.042.

[27] H. Mio, R. Higuchi, W. Ishimaru, A. Shimosaka, Y. Shirakawa, J. Hidaka, Effect of paddle rotational speed on particle mixing behavior in electrophotographic system by using parallel discrete el-

ement method, Advanced Powder Technology 20 (2009) 406–415. doi:10.1016/j.apt.2009.05.002.

[28] J. Hærvig, U. Kleinhans, C. Wieland, H. Spliethoff, A. L. Jensen, K. Sørensen, T. J. Condra, On the adhesive jkr contact and rolling models for reduced particle stiffness discrete element simulations, Powder Technology 319 (2017) 472–482. doi:10.1016/j.powtec.2017.07.006.

[29] T. Kobayashi, T. Tanaka, N. Shimada, T. Kawaguchi, Dem-cfd analysis of fluidization behavior of geldart group a particles using a dynamic adhesion force model, Powder Technology 248 (2013) 143–152. doi:10.1016/j.powtec.2013.02.028.

[30] K. Washino, E. L. Chan, T. Tanaka, Dem with attraction forces using reduced particle stiffness, Powder Technology 325 (2018) 202–208. doi:10.1016/j.powtec.2017.11.024.

[31] S. Chen, W. Liu, S. Li, A fast adhesive discrete element method for random packings of fine particles, Chemical Engineering Science 193 (2019) 336–345. doi:10.1016/j.ces.2018.09.026.

[32] Y. He, A. Hassanpour, M. A. Behjani, A. E. Bayly, A novel stiffness scaling methodology for discrete element modelling of cohesive fine powders, Applied Mathematical Modelling 90 (2021) 817–844. doi:10.1016/j.apm.2020.08.062.

[33] M. Sakai, S. Koshizuka, Large-scale discrete element modeling in pneumatic conveying, Chemical Engineering Science 64 (2009) 533–539. doi:10.1016/j.ces.2008.10.003.

[34] C. Bierwisch, T. Kraft, H. Riedel, M. Moseler, Three-dimensional discrete element models for the granular statics and dynamics of powders in cavity filling, Journal of the Mechanics and Physics of Solids 57 (2009) 10–31.

[35] M. Sakai, H. Takahashi, C. C. Pain, J. P. Latham, J. Xiang, Study on a large-scale discrete element model for fine particles in a fluidized bed, Advanced Powder Technology 23 (2012) 673–681. doi:10.1016/j.apt.2011.08.006.

[36] S. C. Thakur, J. Y. Ooi, H. Ahmadian, Scaling of discrete element model parameters for cohesionless and cohesive solid, Powder Technology 293 (2016) 130–137.

[37] E. L. Chan, K. Washino, Coarse grain model for dem simulation of dense and dynamic particle flow with liquid bridge forces, Chemical Engineering Research and Design 132 (2018) 1060–1069. doi:10.1016/j.cherd.2017.12.033.

[38] K. Washino, E. L. Chan, T. Kaji, Y. Matsuno, T. Tanaka, On large scale cfd–dem simulation for gas–liquid–solid three-phase flows, Particuology 59 (2021) 2–15. doi:10.1016/j.partic.2020.05.006.

[39] M. Sakai, M. Abe, Y. Shigeto, S. Mizutani, H. Takahashi, A. Viré, J. R. Percival, J. Xiang, C. C. Pain, Verification and validation of a coarse grain model of the dem in a bubbling fluidized bed, Chemical Engineering Journal 244 (2014) 33–43. doi:10.1016/j.cej.2014.01.029.

[40] K. Takabatake, Y. Mori, J. G. Khinast, M. Sakai, Numerical investigation of a coarse-grain discrete element method in solid mixing in a spouted bed, Chemical Engineering Journal 346 (2018) 416–426. doi:10.1016/j.cej.2018.04.015.

[41] P. M. Widartiningsih, Y. Mori, K. Takabatake, C. Y. Wu, K. Yokoi, A. Yamaguchi, M. Sakai, Coarse graining dem simulations of a powder die-filling system, Powder Technology 371 (2020) 83–95. doi:10.1016/j.powtec.2020.05.063.

[42] Z. Xie, Y. Shen, K. Takabatake, A. Yamaguchi, M. Sakai, Coarse-grained dem study of solids sedimentation in water, Powder Technology 361 (2020) 21–32. doi:10.1016/j.powtec.2019.11.034.

[43] Y. Mori, M. Sakai, Visualization study on the coarse graining dem for large-scale gas–solid flow systems, Particuology (in press). doi:10.1016/j.partic.2020.07.001.

[44] R. Sun, H. Xiao, Diffusion-based coarse graining in hybrid continuum-discrete solvers: Applications in cfd-dem, In-

ternational Journal of Multiphase Flow 72 (2015) 233–247. doi:10.1016/j.ijmultiphaseflow.2015.02.014.

[45] R. Sun, H. Xiao, Diffusion-based coarse graining in hybrid continuum-discrete solvers: Theoretical formulation and a priori tests, International Journal of Multiphase Flow 77 (2015) 142–157. doi:10.1016/j.ijmultiphaseflow.2015.08.014.

[46] A. D. Renzo, E. Napolitano, F. D. Maio, Coarse-grain dem modelling in fluidized bed simulation: A review, Processes 9 (2021) 279. doi:10.3390/pr9020279.
URL https://www.mdpi.com/2227-9717/9/2/279

[47] E. J. Parteli, J. Schmidt, C. Blümel, K. E. Wirth, W. Peukert, T. Pöschel, Attractive particle interaction forces and packing density of fine glass powders, Scientific Reports 4 (2014) 1–7. doi:10.1038/srep06227.

[48] C. Thornton, Interparticle sliding in the presence of adhesion, Journal of Physics D: Applied Physics 24 (1991) 1942–1946. doi:10.1088/0022-3727/24/11/007.

[49] J. S. Marshall, Discrete-element modeling of particulate aerosol flows, Journal of Computational Physics 228 (2009) 1541–1561. doi:10.1016/j.jcp.2008.10.035.

[50] C. D. Willett, M. J. Adams, S. A. Johnson, J. P. Seville, Capillary bridges between two spherical bodies, Langmuir 16 (2000) 9396–9405. doi:10.1021/la000657y.

[51] G. Lian, C. Thornton, M. J. Adams, A theoretical study of the liquid bridge forces between two rigid spherical bodies, Journal of Colloid And Interface Science 161 (1993) 138–147. doi:10.1006/jcis.1993.1452.

[52] D. Tabor, Surface forces and surface interactions, Journal of Colloid And Interface Science 58 (1977) 2–13. doi:10.1016/0021-9797(77)90366-6.

[53] M. Pasha, C. Hare, A. Hassanpour, M. Ghadiri, Analysis of ball indentation on cohesive powder beds using distinct element modelling, Powder Technology 233 (2013) 80–90. doi:10.1016/j.powtec.2012.08.017.

[54] J. S. Ramaker, M. A. Jelgersma, P. Vonk, N. W. F. Kossen, Scale-down of a high-shear pelletisation process: Flow profile and growth kinetics, International Journal of Pharmaceutics 166 (1998) 89–97.

[55] E. L. Chan, K. Washino, G. K. Reynolds, B. Gururajan, M. J. Hounslow, A. D. Salman, Blade-granule bed stress in a cylindrical high shear granulator: Further characterisation using dem, Powder Technology 300 (2016) 92–106. doi:10.1016/j.powtec.2016.02.010.

List of Figures

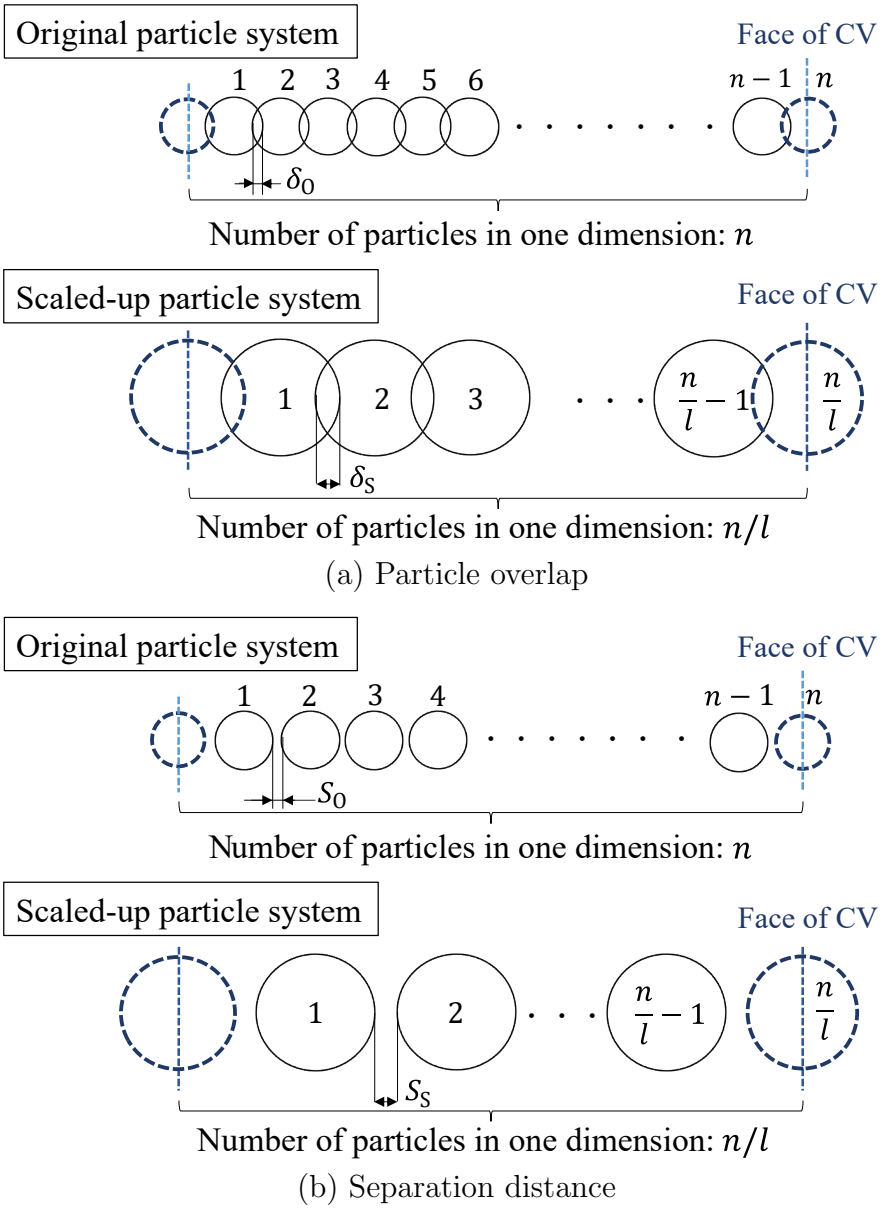

(a) Particle overlap

(b) Separation distance

Figure 1: Geometric similarity in control volume (1-dimension).

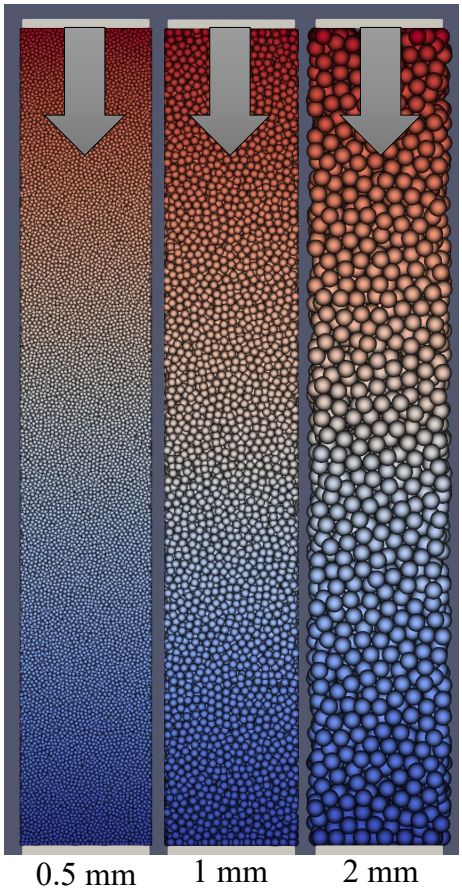

Figure 2: Uniaxial compression of packed particle bed using the proposed method. Periodic boundaries are used in the lateral directions. Colour indicates the particle velocity magnitude between 0 mm/s (blue) and 5 mm/s (red).

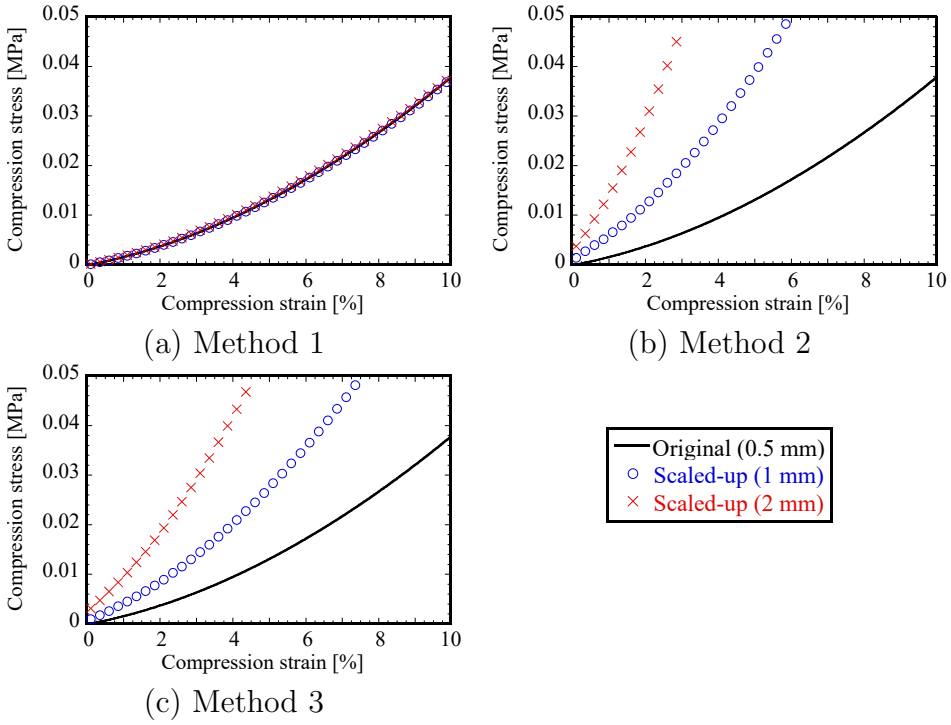

Figure 3: Stress-strain relationship during uniaxial compression of packed particle bed.

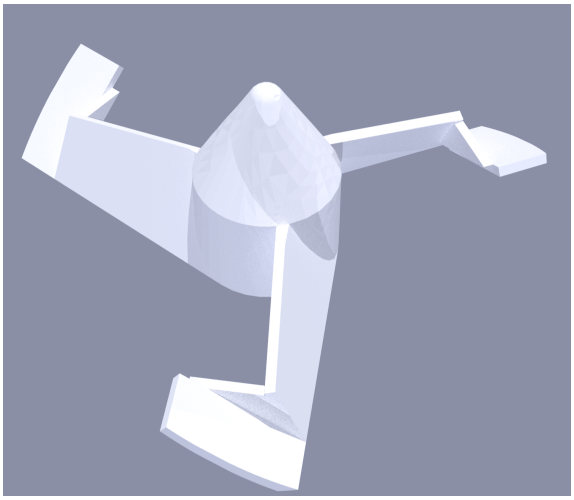

Figure 4: Snapshot of the impeller of vertical mixer.

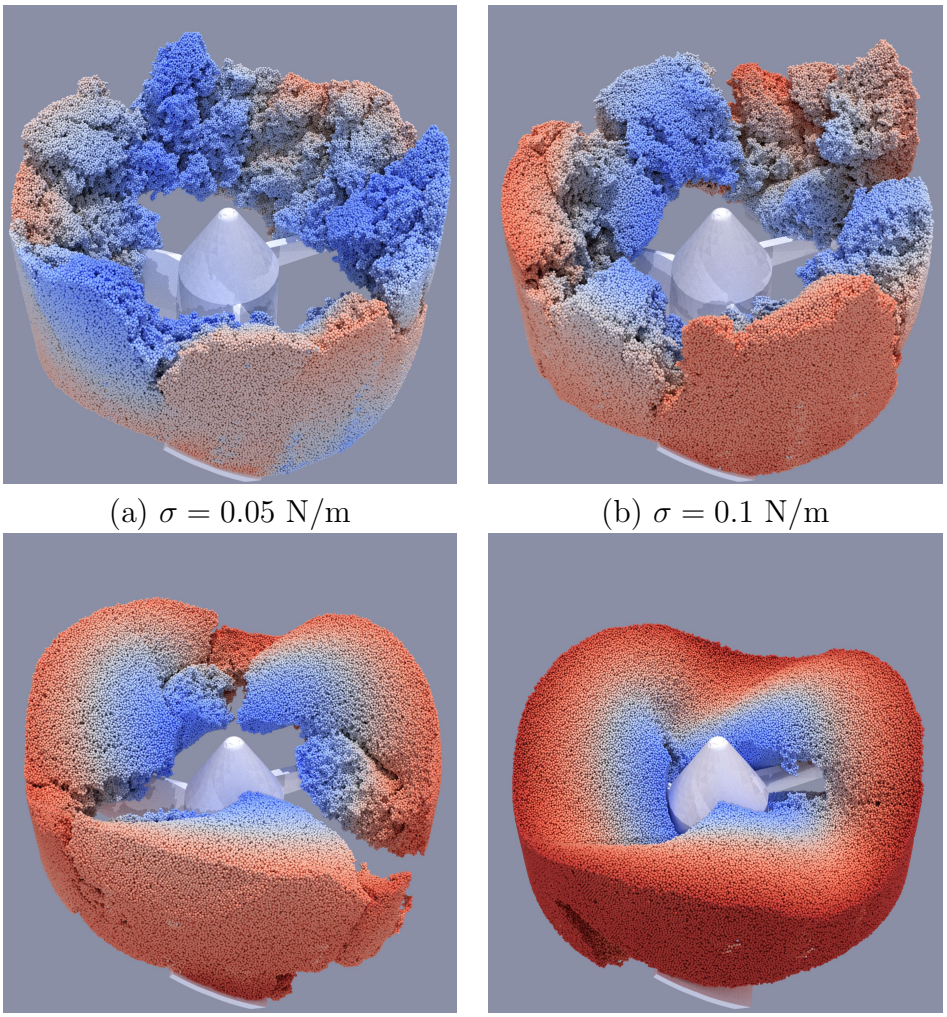

(a) $\sigma = 0.05$ N/m (b) $\sigma = 0.1$ N/m

(c) $\sigma = 0.2$ N/m (d) $\sigma = 0.4$ N/m

Figure 5: Snapshots of the original particles in vertical mixer with capillary force. Colour indicates the particle velocity magnitude between 0 m/s (blue) and 1.4 m/s (red).

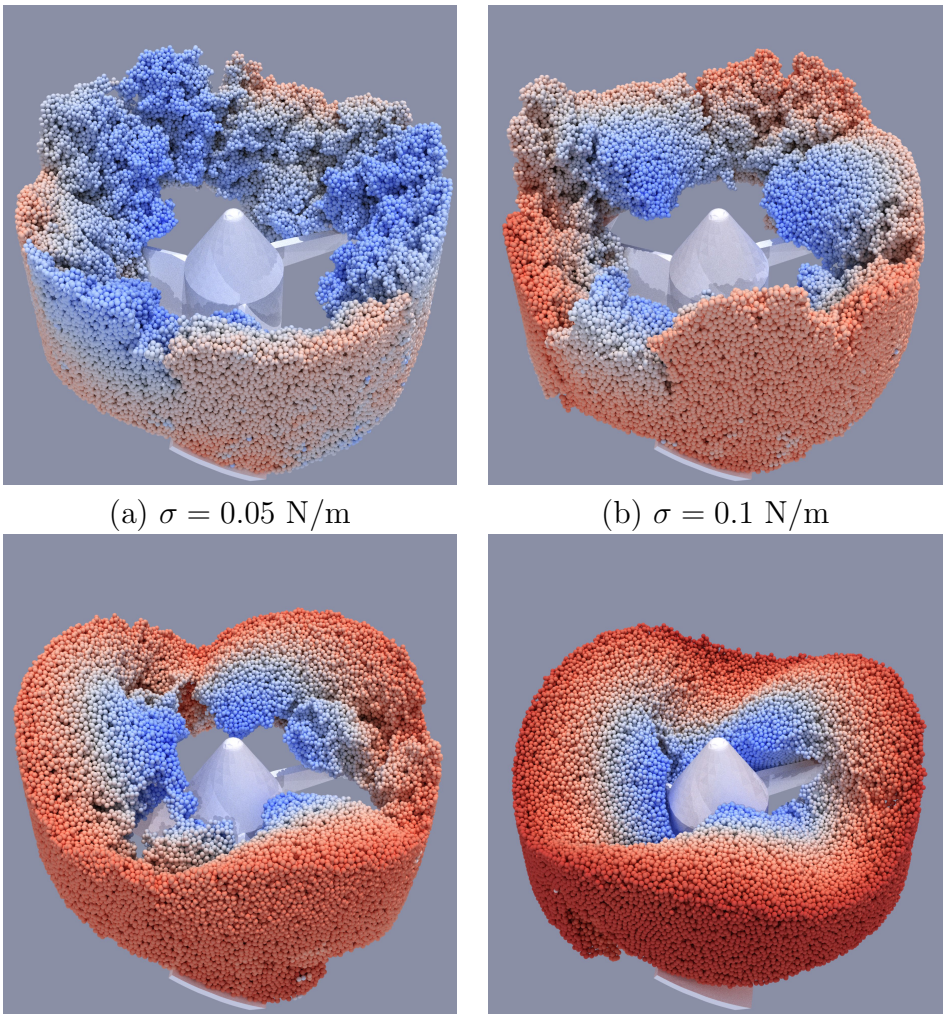

(a) $\sigma = 0.05$ N/m (b) $\sigma = 0.1$ N/m

(c) $\sigma = 0.2$ N/m (d) $\sigma = 0.4$ N/m

Figure 6: Snapshots of the scaled-up particles in vertical mixer with capillary force (scale factor = 2, Method 1). Colour indicates the particle velocity magnitude between 0 m/s (blue) and 1.4 m/s (red).

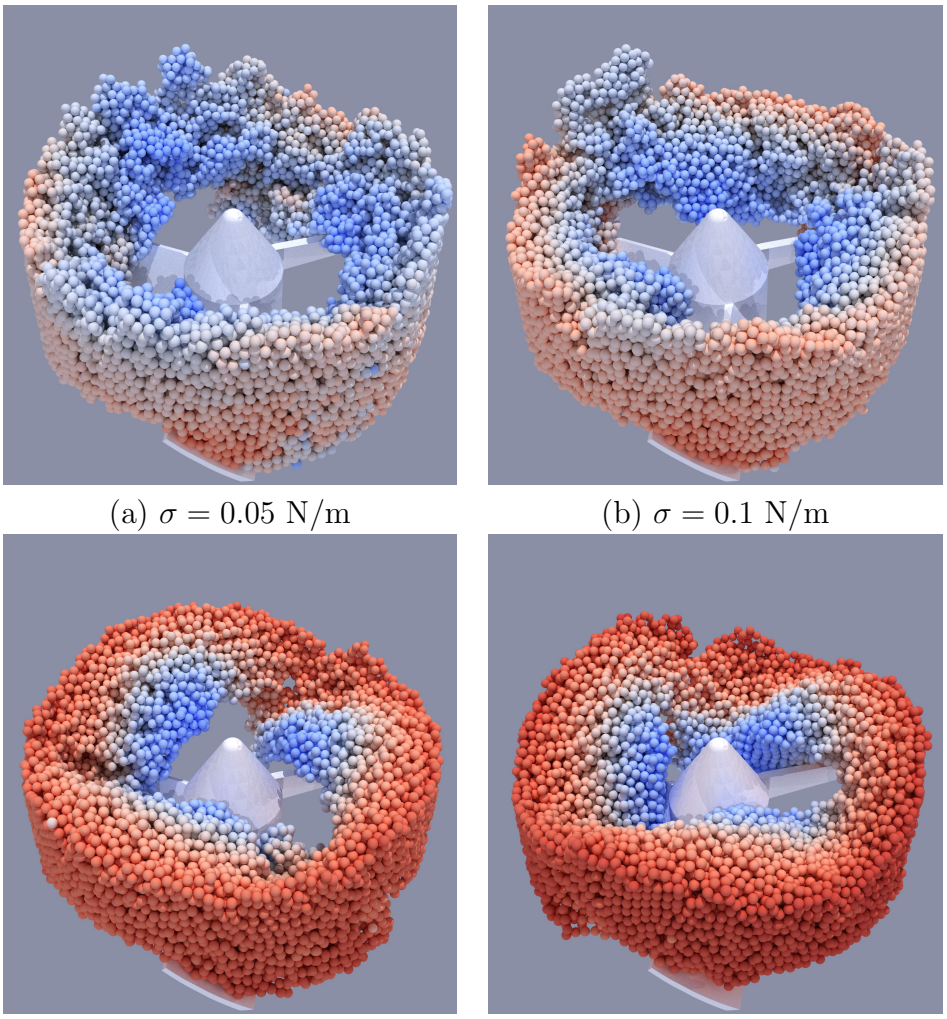

(a) $\sigma = 0.05$ N/m (b) $\sigma = 0.1$ N/m

(c) $\sigma = 0.2$ N/m (d) $\sigma = 0.4$ N/m

Figure 7: Snapshots of the scaled-up particles in vertical mixer with capillary force (scale factor = 4, Method 1). Colour indicates the particle velocity magnitude between 0 m/s (blue) and 1.4 m/s (red).

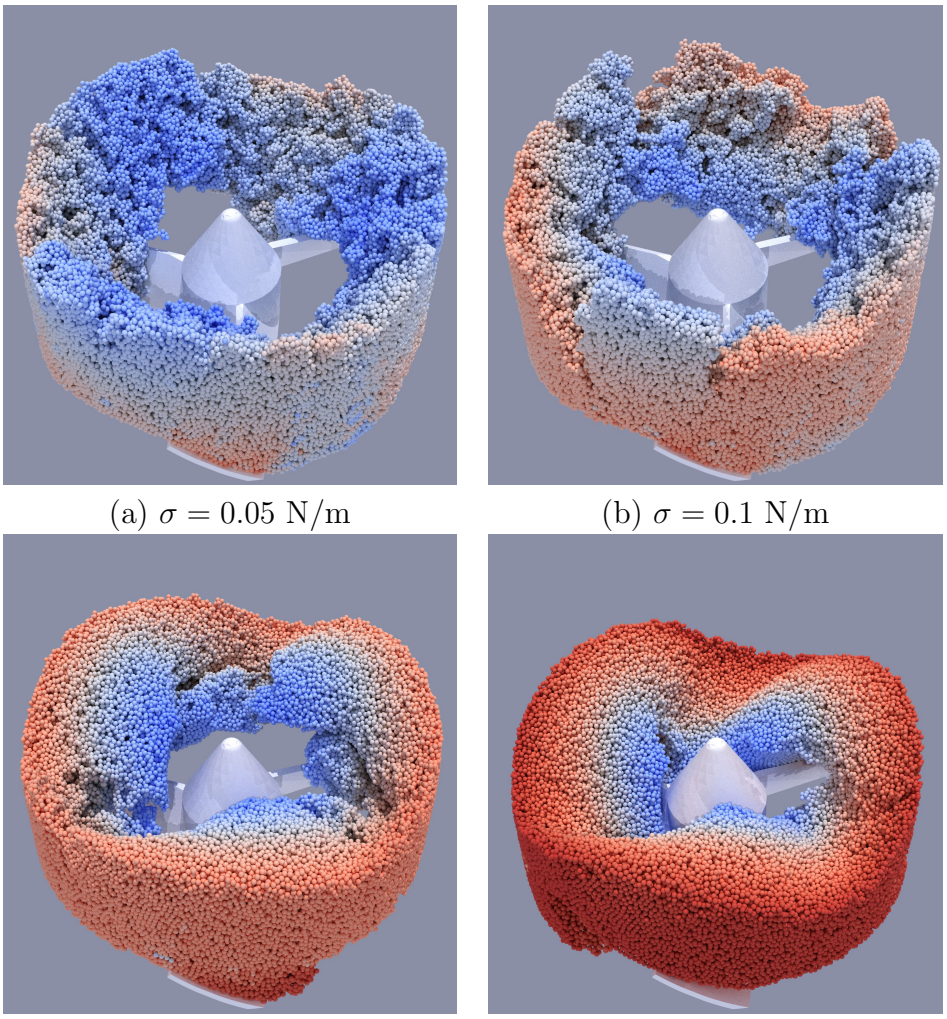

(a) $\sigma = 0.05$ N/m (b) $\sigma = 0.1$ N/m

(c) $\sigma = 0.2$ N/m (d) $\sigma = 0.4$ N/m

Figure 8: Snapshots of the scaled-up particles in vertical mixer with capillary force (scale factor = 2, Method 2). Colour indicates the particle velocity magnitude between 0 m/s (blue) and 1.4 m/s (red).

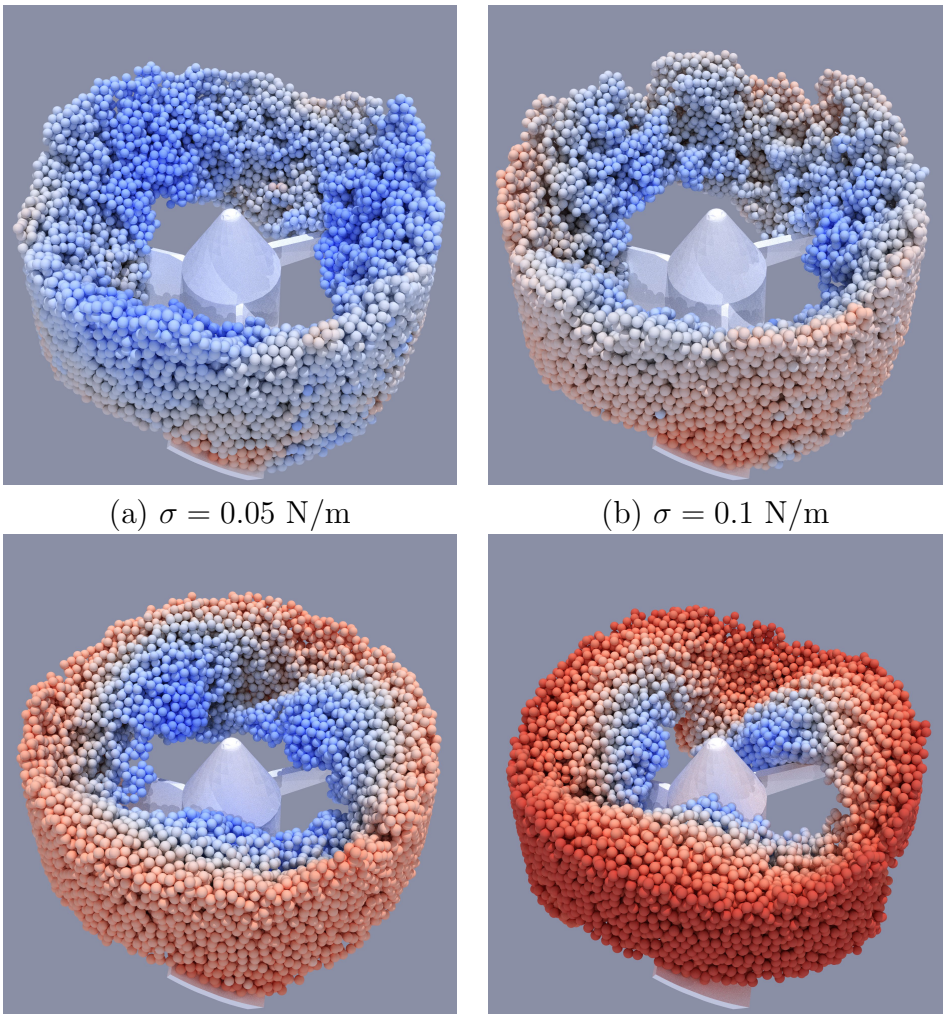

(a) $\sigma = 0.05$ N/m (b) $\sigma = 0.1$ N/m

(c) $\sigma = 0.2$ N/m (d) $\sigma = 0.4$ N/m

Figure 9: Snapshots of the scaled-up particles in vertical mixer with capillary force (scale factor = 4, Method 2). Colour indicates the particle velocity magnitude between 0 m/s (blue) and 1.4 m/s (red).

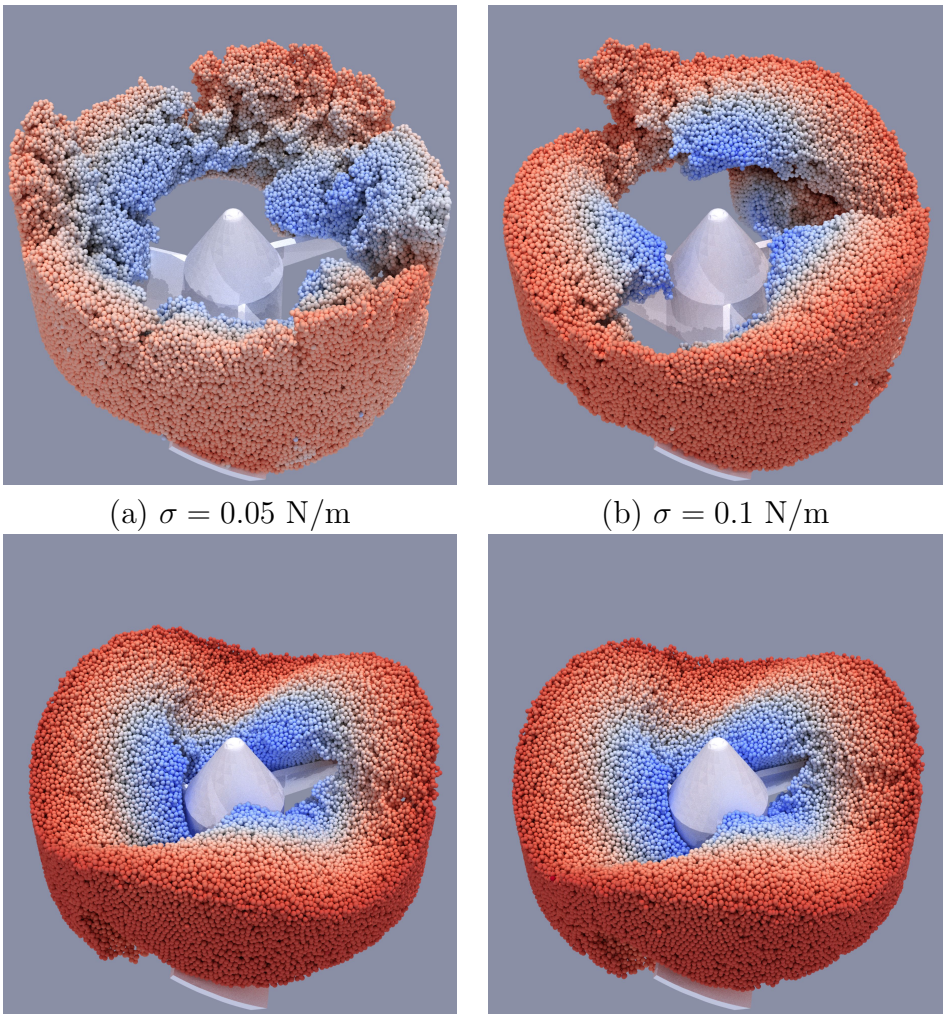

(a) $\sigma = 0.05$ N/m (b) $\sigma = 0.1$ N/m

(c) $\sigma = 0.2$ N/m (d) $\sigma = 0.4$ N/m

Figure 10: Snapshots of the scaled-up particles in vertical mixer with capillary force (scale factor = 2, Method 3). Colour indicates the particle velocity magnitude between 0 m/s (blue) and 1.4 m/s (red).

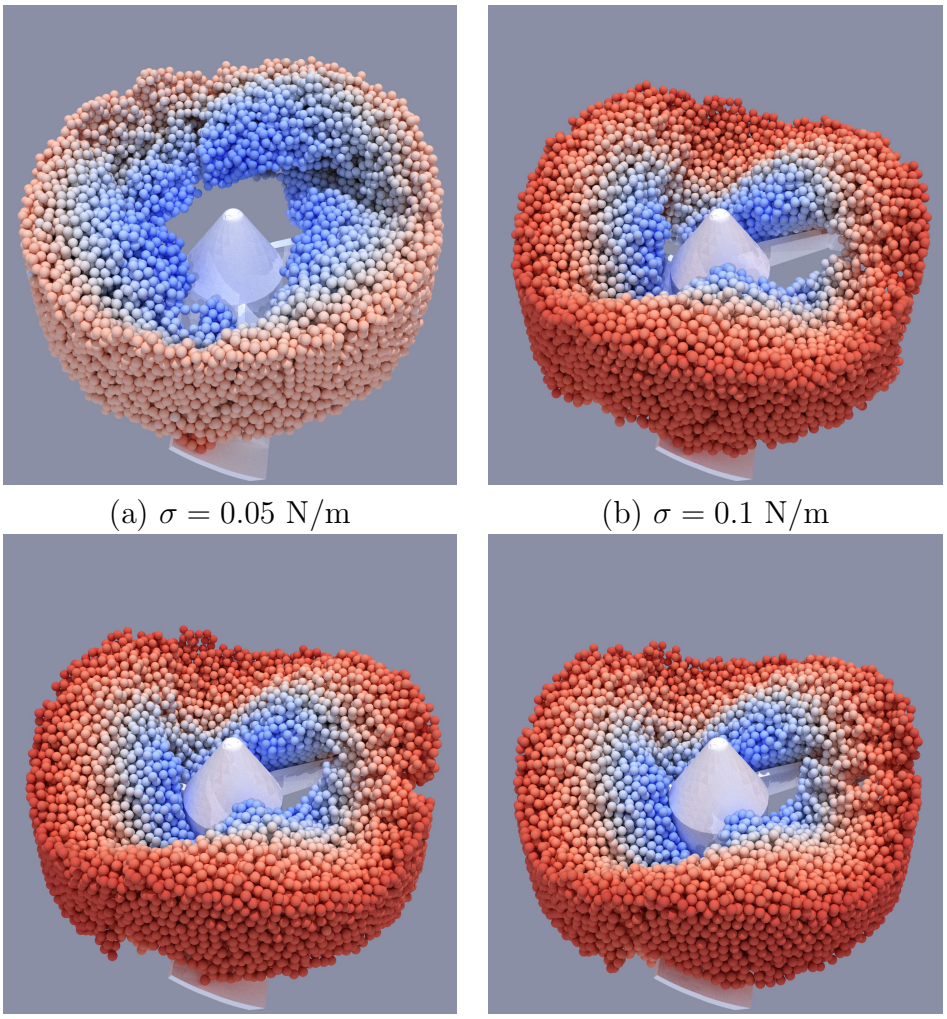

(a) $\sigma = 0.05$ N/m (b) $\sigma = 0.1$ N/m

(c) $\sigma = 0.2$ N/m (d) $\sigma = 0.4$ N/m

Figure 11: Snapshots of the scaled-up particles in vertical mixer with capillary force (scale factor = 4, Method 3). Colour indicates the particle velocity magnitude between 0 m/s (blue) and 1.4 m/s (red).

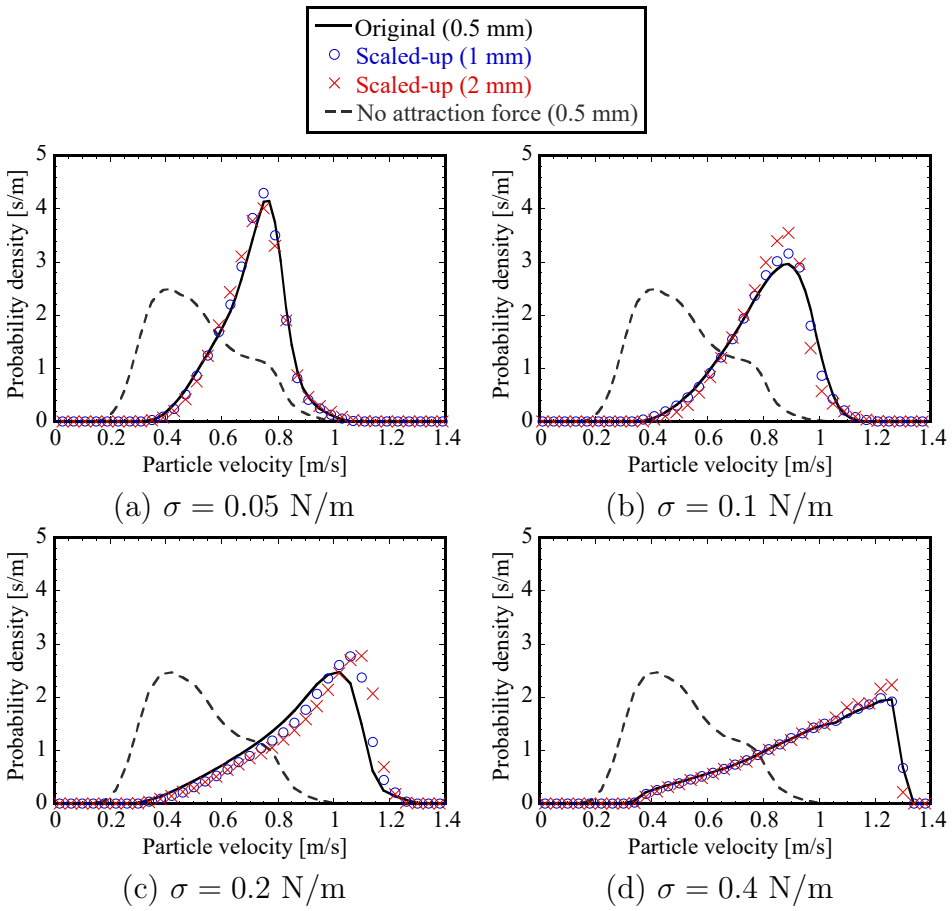

Figure 12: Probability density distribution of particle velocity magnitude in vertical mixer with capillary force (Method 1).

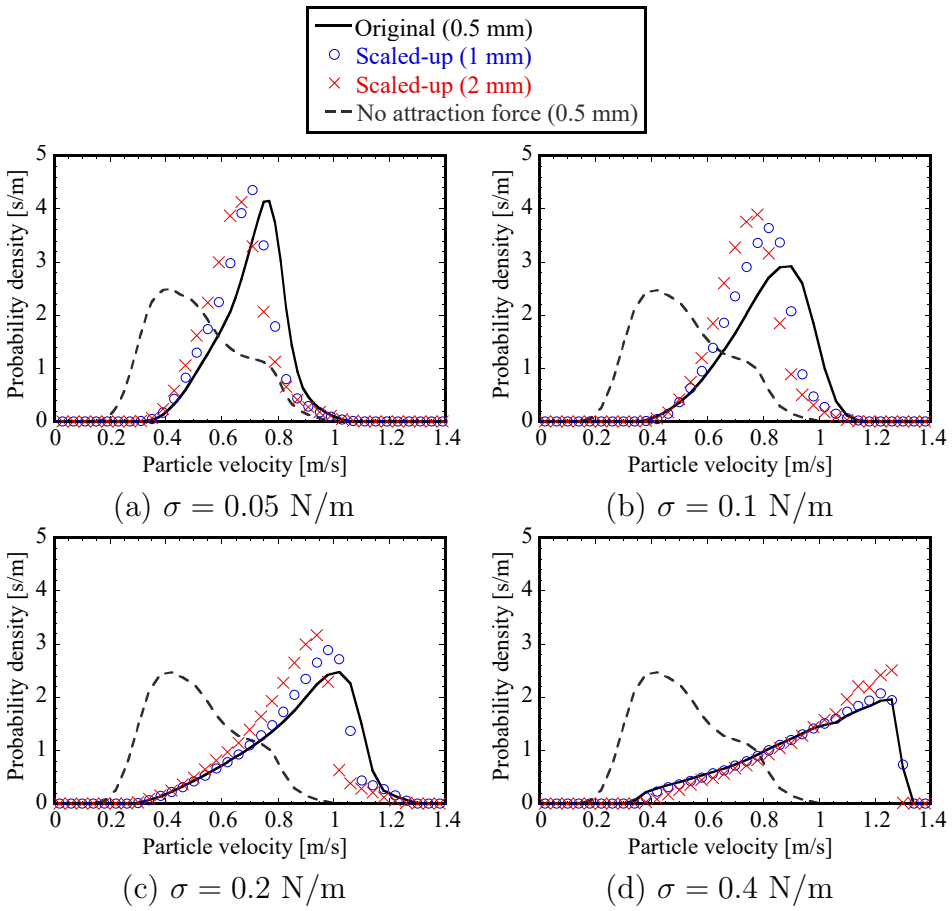

Figure 13: Probability density distribution of particle velocity magnitude in vertical mixer with capillary force (Method 2).

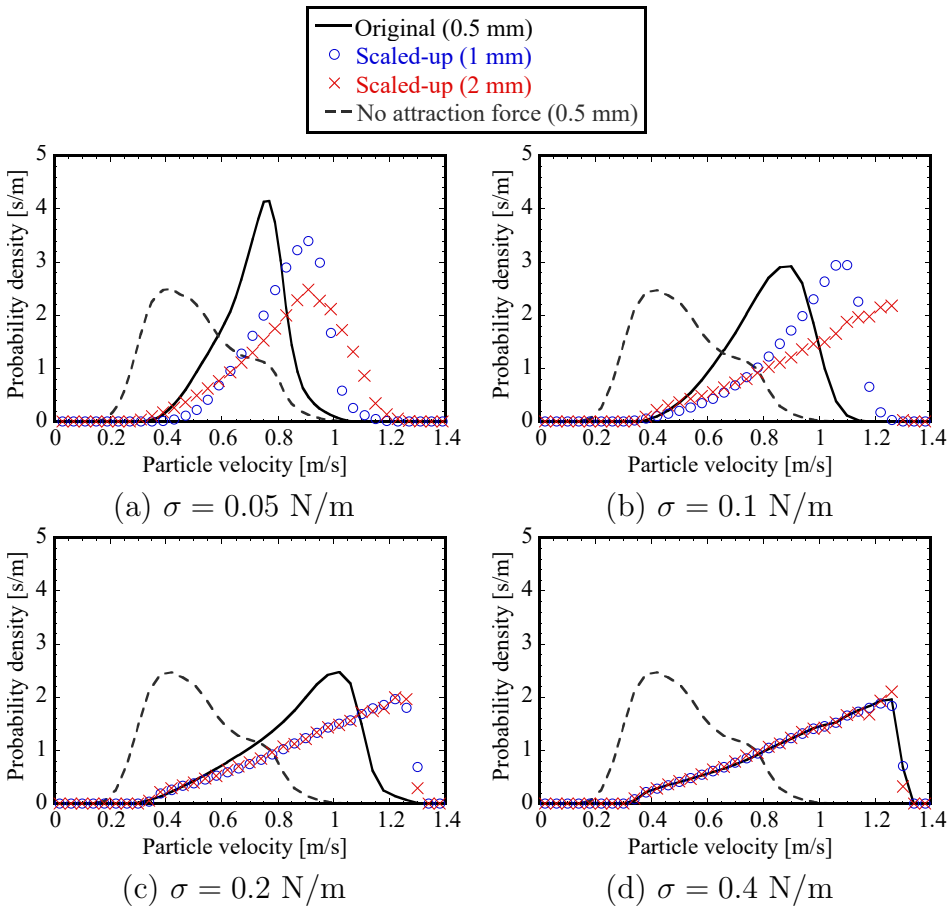

Figure 14: Probability density distribution of particle velocity magnitude in vertical mixer with capillary force (Method 3).

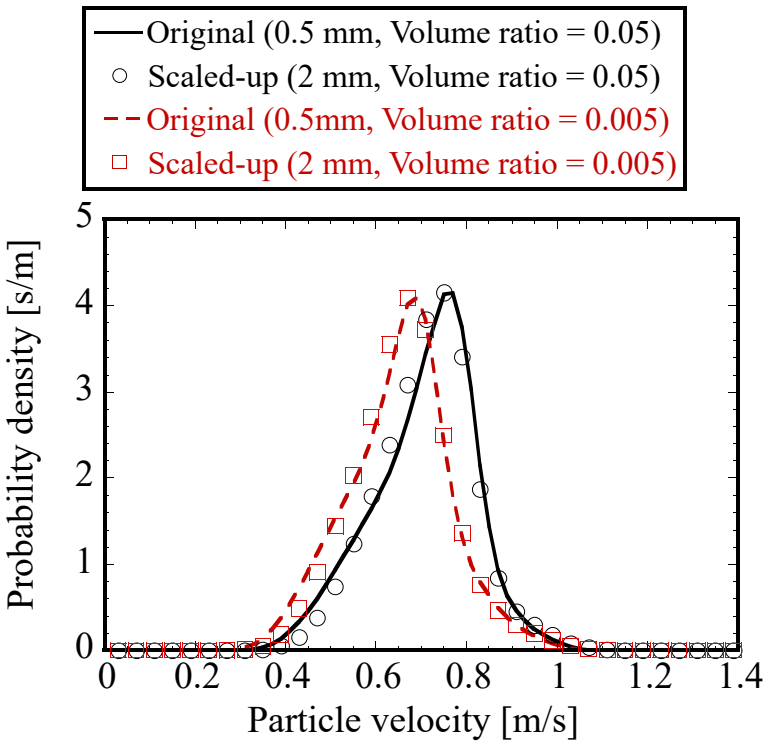

Figure 15: Probability density distribution of particle velocity magnitude in vertical mixer with capillary force using different liquid to solid volume ratios (Method 1, $\sigma = 0.05$ N/m).

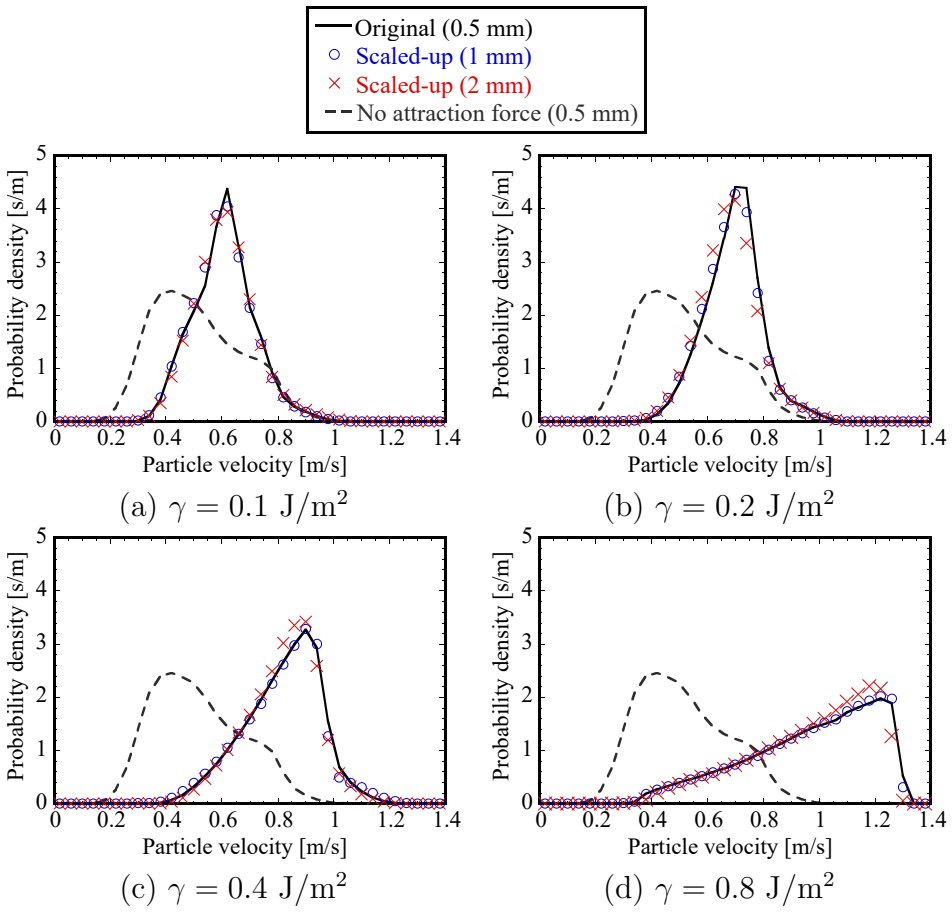

Figure 16: Probability density distribution of particle velocity magnitude in vertical mixer with JKR surface adhesion force (Method 1).

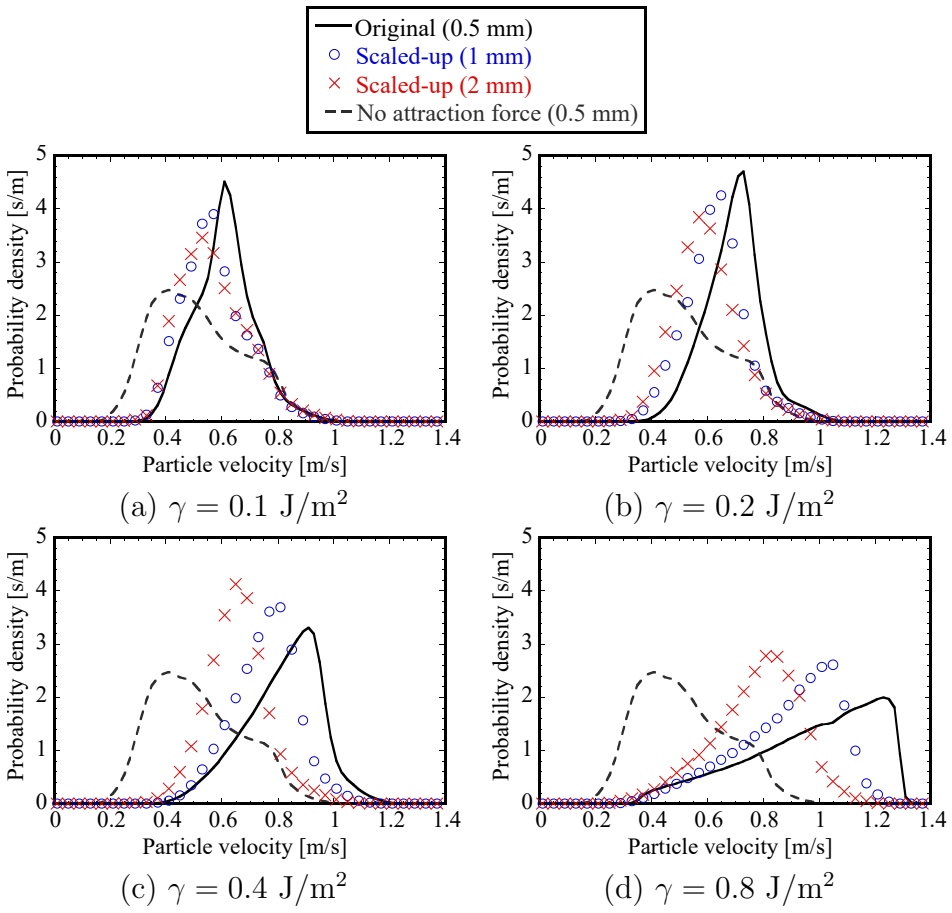

Figure 17: Probability density distribution of particle velocity magnitude in vertical mixer with JKR surface adhesion force (Method 2).

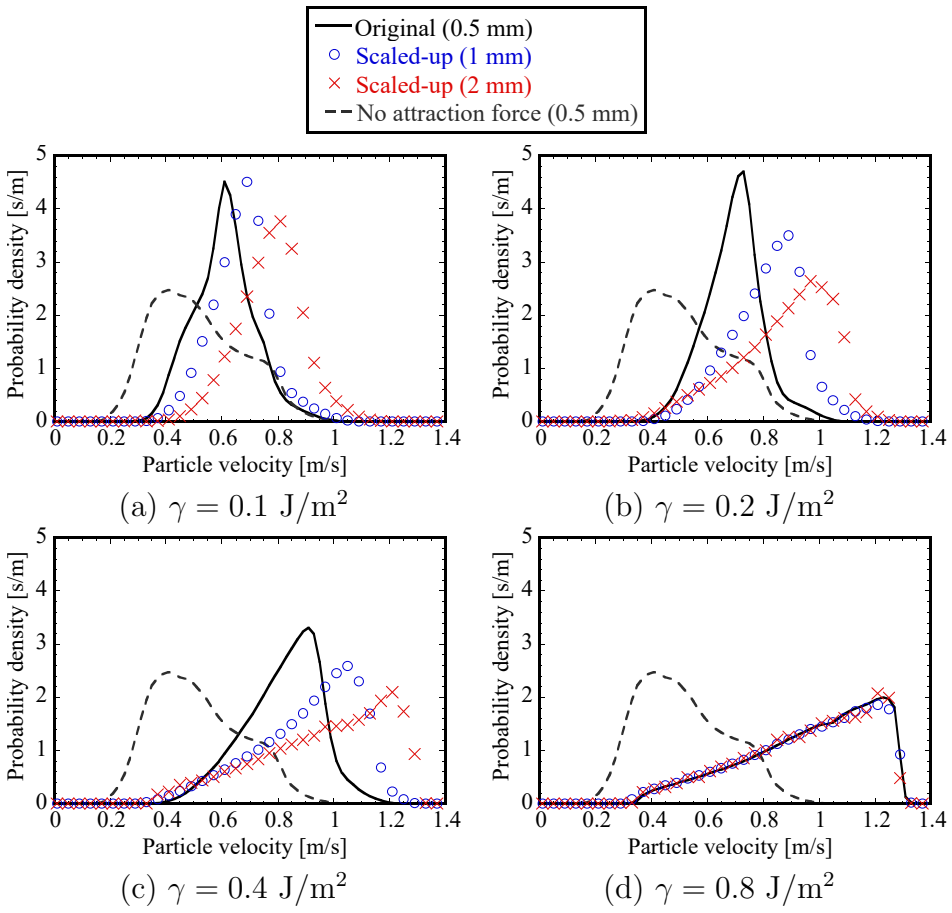

Figure 18: Probability density distribution of particle velocity magnitude in vertical mixer with JKR surface adhesion force (Method 3).

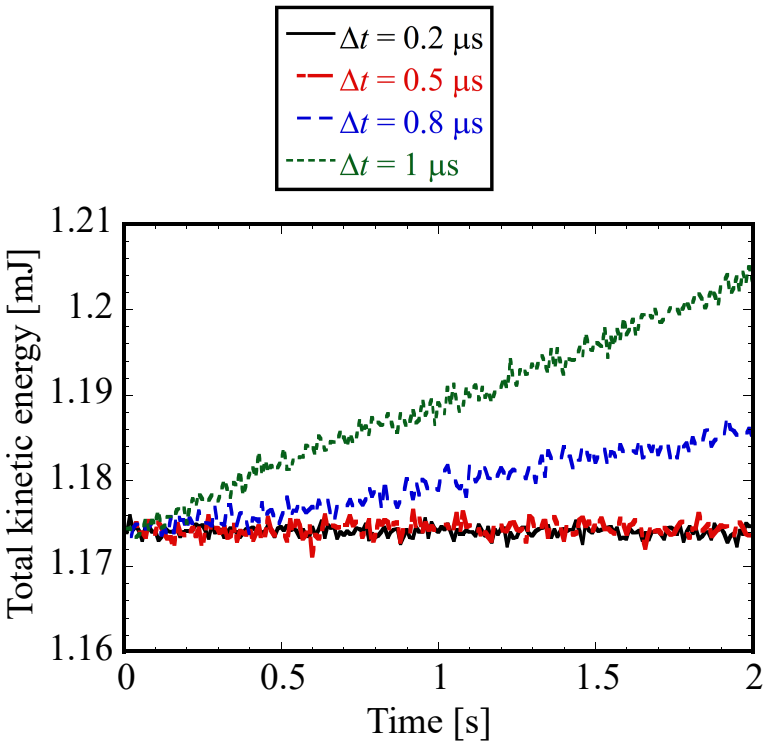

Figure 19: Temporal change of total kinetic energy of original particles in periodic box.

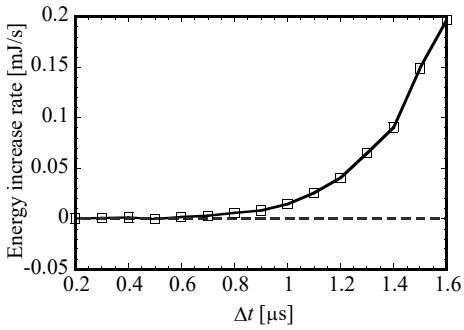

(a) Original (0.5 mm)

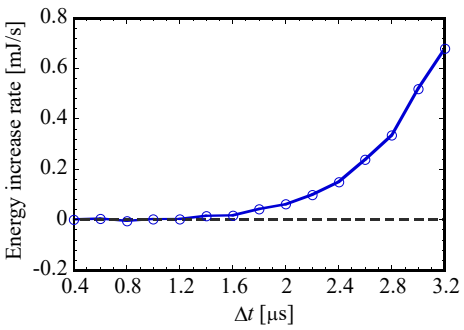

(b) Scaled-up (1 mm)

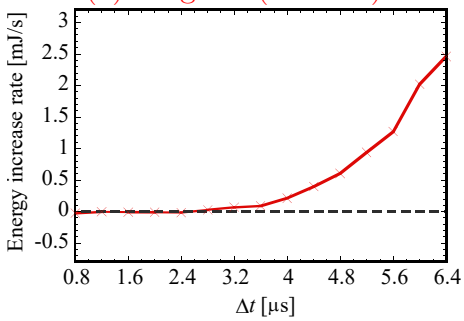

(c) Scaled-up (2 mm)

Figure 20: Increase rate of total kinetic energy in periodic box as a function of time step.

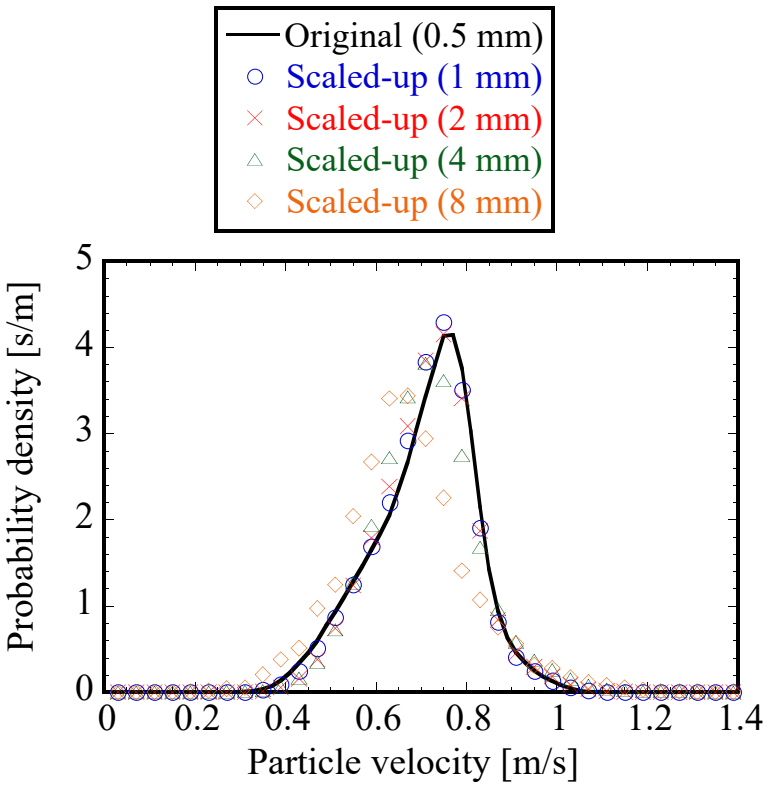

Figure 21: Probability density distribution of particle velocity magnitude in vertical mixer with capillary force including the larger scale factor results (Method 1, $\sigma = 0.05$ N/m).

List of Tables

Table 1: Scale power indices of Sakai and Koshizuka and Sakai et al. [33, 35].

Scale power index	Force / torque type	Classification
4	Torque	Interparticle
3	Gravity	Body
3	Fluid force	Body
3	Contact force	Interparticle
2	van der Waals force	Interparticle

Table 2: Scale power indices of Chan and Washino and Washino et al. [37, 38].

Scale power index	Force / torque type	Classification
3	Gravity	Body
3	Fluid force	Body
2	Contact force	Interparticle
2	Capillary force	Interparticle
2	Viscous force	Interparticle
2	Torque	Interparticle

Table 3: Relationships of the original and scaled-up variables.

Variable	Previous work [33, 35, 37, 38]	Present work
Translational velocity	$\boldsymbol{v}_{\mathrm{O}} = \boldsymbol{v}_{\mathrm{S}}$	$\boldsymbol{v}_{\mathrm{O}} = \boldsymbol{v}_{\mathrm{S}}$
Rotational velocity	$\boldsymbol{\omega}_{\mathrm{O}} = l\boldsymbol{\omega}_{\mathrm{S}}$	$\boldsymbol{\omega}_{\mathrm{O}} = l\boldsymbol{\omega}_{\mathrm{S}}$
Particle overlap	$\delta_{\mathrm{O}} = \delta_{\mathrm{S}}$	$\delta_{\mathrm{O}} = \delta_{\mathrm{S}}/l$
Separation distance	$S_{\mathrm{O}} = S_{\mathrm{S}}$	$S_{\mathrm{O}} = S_{\mathrm{S}}/l$

Table 4: Methods used in scaled-up particle simulations.

Method 1	Method 2	Method 3
$\boldsymbol{F}_{I\mathrm{S}} = l^2 \boldsymbol{F}_{I\mathrm{O}}$	$\boldsymbol{F}_{I\mathrm{S}} = l^2 \boldsymbol{F}_{I\mathrm{O}}$	$\boldsymbol{F}_{I\mathrm{S}} = l^3 \boldsymbol{F}_{I\mathrm{O}}$
$\boldsymbol{M}_{I\mathrm{S}} = l^2 \boldsymbol{M}_{I\mathrm{O}}$	$\boldsymbol{M}_{I\mathrm{S}} = l^2 \boldsymbol{M}_{I\mathrm{O}}$	$\boldsymbol{M}_{I\mathrm{S}} = l^3 \boldsymbol{M}_{I\mathrm{O}}$
$\boldsymbol{F}_{B\mathrm{S}} = l^3 \boldsymbol{F}_{B\mathrm{O}}$	$\boldsymbol{F}_{B\mathrm{S}} = l^3 \boldsymbol{F}_{B\mathrm{O}}$	$\boldsymbol{F}_{B\mathrm{S}} = l^3 \boldsymbol{F}_{B\mathrm{O}}$
$\delta_{\mathrm{O}} = \delta_{\mathrm{S}}/l$	$\delta_{\mathrm{O}} = \delta_{\mathrm{S}}$	$\delta_{\mathrm{O}} = \delta_{\mathrm{S}}/l$
$S_{\mathrm{O}} = S_{\mathrm{S}}/l$	$S_{\mathrm{O}} = S_{\mathrm{S}}$	$S_{\mathrm{O}} = S_{\mathrm{S}}/l$

Table 5: Original particle properties for uniaxial compression of packed particle bed.

Property	Value
Particle diameter [mm]	0.5
Particle density [kg/m^3]	2500
Initial bed height [mm]	100
Young's modulus [MPa]	5
Poisson's ratio [-]	0.3
Restitution coefficient [-]	0.9
Sliding friction coefficient [-]	0.3

Table 6: Common properties of original particles for vertical mixer.

Property	Value
Particle diameter [mm]	0.5
Particle density [kg/m^3]	1000
Total mass [kg]	0.0458
Young's modulus [MPa]	100
Poisson's ratio [-]	0.3
Restitution coefficient [-]	0.1
Sliding friction coefficient [-]	0.3

Table 7: Original particle properties of periodic box simulation.

Property	Value
Particle diameter [mm]	0.5
Particle density [kg/m^3]	1000
Number of particles [-]	36644
Young's modulus [MPa]	100
Poisson's ratio [-]	0.3
Restitution coefficient [-]	1
Sliding friction coefficient [-]	0